

<sub>1</sub>      Proposal for a Full-Scale Detector Engineering Test  
<sub>2</sub>      and Test Beam Calibration of a Single-Phase LAr  
<sub>3</sub>      TPC

<sub>4</sub>      A. name1<sup>1</sup>, B. name2<sup>2</sup>, and C. name3<sup>3</sup>

<sub>5</sub>      <sup>1</sup>Department of X1, University Y1

<sub>6</sub>      <sup>2</sup>Department of X2, University Y2

<sub>7</sub>      <sup>3</sup>Department of X3, University YY3

<sub>8</sub>      March 8, 2015

<sub>9</sub>      **Abstract**

<sub>10</sub>     insert abstract here

# 11 Contents

12	<b>1 Introduction</b> [~5 pages; <b>Thomas/Greg/Bob Wilson</b> ]	3
13	1.1 Physics goals of LBNF . . . . .	3
14	1.2 Single-phase LAr TPC Prototype . . . . .	3
15	1.3 Goals for the prototype run . . . . .	4
16	<b>2 CERN prototype detector and charged particle beam test</b> [~10 pages; <b>Donna/Jarek</b> ]	4
18	2.1 Requirements for the detector, beam and commissioning . . . . .	5
19	2.2 Detector performance tests . . . . .	9
20	2.3 Other measurements . . . . .	11
21	<b>3 Single Phase LAr Detector</b> [~10 pages; <b>J. Stewart et al.</b> ]	11
22	3.1 LBNF detector . . . . .	11
23	3.2 CERN prototype detector . . . . .	13
24	<b>4 Cryostat and cryogenics system</b> [~5 pages; <b>David/Barry/Jack</b> ]	27
25	4.1 LBNF detector . . . . .	27
26	4.2 CERN prototype detector . . . . .	27
27	4.3 Cryogenic System (from David Montanari) . . . . .	37
28	<b>5 Charged Particle Test Beam Requirements</b> [~10 pages; <b>Cheng-Ju</b> ]	39
29	5.1 Particle Beam Requirements . . . . .	39
30	5.2 EHN1 H4ext Beamlne . . . . .	39
31	5.3 Beam Instrumentation . . . . .	41
32	5.4 Muon Beam Halo Counters . . . . .	41
33	5.5 Beam Window on LAr Cryostat . . . . .	41
34	<b>6 Computing requirements, data handling and software</b> [~3 pages; <b>Maxim Potekhin/Craig Tull ]</b>	41
35	6.1 Overview . . . . .	41
36	6.2 Collecting and Storing Raw Data . . . . .	42
37	6.3 Databases . . . . .	44
38	6.4 A note on Simulation and Reconstruction Software . . . . .	44
39	6.5 Distributed Computing, Workload and Workflow Management . . . . .	45
41	<b>7 CERN neutrino platform test environment</b> [5 pages; <b>David/Jack/Cheng-Ju/Thomas</b> ]	47
42		47
43	<b>8 Organization, schedule and cost estimate</b> [~5 pages; <b>Thomas/Greg</b> ]	47
44	<b>9 Summary</b> [~2 pages; <b>Thomas/Greg</b> ]	47

45 **1 Introduction** [~5 pages; Thomas/Greg/Bob Wil-  
46 son]

47 This document is a technical report for the Expression of Interest <reference> submitted  
48 to the CERN SPSC in October 2014. In this report, we detail the proposal to test full-  
49 scale detector elements for a single-phase liquid argon (LAr) TPC based on the former  
50 LBNE design which is a potential viable technology for use as a far detector for the  
51 experiment that will be at the Long Baseline Neutrino Facility (LBNF). To mitigate  
52 the risks associated with extrapolating small scale versions of the single-phase LAr TPC  
53 technology to a full-scale detector element, it is essential to benchmark the operation of a  
54 full-scale detector elements in a particle beam. The beam facility at the CERN Neutrino  
55 Platform (cite) provides an opportunity to perform this crucial test of the proposed  
56 single-phase LAr TPC and inform the decision regarding phased implementation of the  
57 far detector for LBNF.

58 **1.1 Physics goals of LBNF**

59 An international collaboration is forming that will utilize a proposed 1.2 MW proton  
60 beam at FNAL to create a neutrino beam that will be directed at the Homestake Mine  
61 in the USA. The proposal is to place by the year 2024 <mention 2021 date for 10kton>  
62 a 40 kton LAr TPC in the underground facility at Homestake to observe the oscillation  
63 of  $\nu_\mu \rightarrow \nu_e$  and  $\bar{\nu}_\mu \rightarrow \bar{\nu}_e$  that occur near a neutrino energy of 3 GeV and thereby make  
64 precision measurements of  $\delta_{CP}$ ,  $\delta_{13}$ , and  $\delta_{23}$  and determining the neutrino mass hierarchy.  
65 In order to make such precise measurements, the detector will need to accurately identify  
66 and measure the energy of the particles produced in the neutrino interaction with Argon  
67 which will range from a few GeV to hundreds of MeV.

68 **1.2 Single-phase LAr TPC Prototype**

69 The LBNE-style single-phase LAr TPC is design to be scalable using module units that  
70 consist of a factory-built anode plane, a cathode a plane, and a field cage with the anode  
71 plane assemblies measuring 6.0m (h)  $\times$  2.3m (w)  $\times$  0.09m (d) and a drift length of 2.5m.  
72 The electronics will be mounted in the cryostat on the wire planes to reduce the number  
73 of cables that penetrate the cryostat and optimize the electronic signal to noise. Event  
74 timing will be determined through the use of scintillation photon detectors that will use  
75 light collection paddles. With this modular design as shown in <insert figure of LBNE  
76 detector to shown modular design> , it will be possible to achieve the goal of 40 kton  
77 detector for the LBNF far site.

78 Some features of this single-phase design will be tested using smaller scale prototypes  
79 such as the ongoing tests with a 35ton unit at Fermilab and the 5ton CAPTAIN LAr  
80 TPC. However, none of these smaller prototypes uses full scale detector elements or  
81 are large enough to fully contain particles. Considering that the detector at the LBNF  
82 far site will be about a factor of 50 larger in scale than the ICARUS detector which  
83 is currently the largest LAr TPC detector built to date, it is essential to validate the  
84 full-scale detector elements in a particle beam at the CERN Neutrino Platform.

85 In order to fully contain particles within the energy range of interest and provide  
86 space for detector services, the cryostat will need to have a minimum inner dimensions  
87 of 8.4m (h)  $\times$  7.3m (w)  $\times$  9.5m (d). It is anticipated that the CERN Neutrino Platform  
88 will facilitate the design and construction of the cryostat and that this effort will common  
89 area that will motivate collaboration with the WA105 team.

### 90 1.3 Goals for the prototype run

91 The goals of the prototype run include:

- 92 • Use of particle beam to assess
  - 93 tracking and calorimetric response
  - 94 reconstruction algorithm
  - 95 Monte Carlo simulation
  - 96 Secondary hadron interactions in detector
- 97 • Verifying argon contamination mitigation
- 98 • Full-scale structural test under LAr cryogenic conditions
- 99 • Verification of TPC Electrics under LAr cryogenic conditions
- 100 • Study light levels of the photon detection system
- 101 • Developing installation procedures for full-scale electronics

## 102 2 CERN prototype detector and charged particle 103 beam test [~10 pages; **Donna/Jarek**]

### 104 TODO list

105 **Sensitivity plots.** Create plots for the CPV and HM sensitivities for 40kton detector  
106 and 1.2 MW beam. Plots should include various combinations of the assumed  
107 uncertainties: with current best measurements, with best guesses about uncer-  
108 tainties we can archive and with uncertainties which will be obtain using beam  
109 test experiment at CERN.

110 **E-m shower calibration energy scale.** Estimate statistics of particles to optimise  
111 the measurement of EM showers. Provide the necessary statistics as a function of  
112 energy. Optimise the energy bins widths, where we expect coarser bins for higher  
113 energies than for lower energies.

114 **Hadronic shower calibration** Estimate statistics of particles to optimise the mea-  
115 surement of hadronic showers. Provide the necessary statistics as a function of  
116 energy. Optimise the energy bins widths, were we expect coarser bins for higher  
117 energies than for lower energies.

118 Estimate pi0 production from the proton scattering in the TPC.

- 119 **Reconstruction issues.** Obtain values for the uncertainties due to finding vertex po-  
 120 sition of neutrino interactions.  
 121 Estimate statistics necessary to improve low energy electrons acceptance due to  
 122 reconstruction algorithms limitations.  
 123 **e/gamma separation** Estimate statistics necessary for improvement of the e/gamma  
 124 separation. Assume three values for wire pitch: 3mm, 4mm and 5mm.  
 125 **Pion cross sections: absorption, charge exchange in Ar** Get statistics for pions  
 126 to measure their cross sections. Estimate energy bin widths.  
 127 **Kaon cross section in Ar** Get statistics for kaons to measure their cross sections.  
 128 Estimate energy bin widths.  
 129 **Muon capture** Estimate statistics for antimuons for capture on argon to be used for  
 130 the statistical determination of the wrong sign neutrino contribution on the beam.

## 131 **2.1 Requirements for the detector, beam and commissioning**

132 The Single-Phase Cern Prototype detector is intended to provide necessary information  
 133 to reduce systematic uncertainties for the oscillation measurements in the US-based  
 134 long base-line neutrino experiment. The LAr TPC technology is not new but wasn't  
 135 extensively used in the 1-10 GeV neutrino energy range. The main source of uncertainties  
 136 due to detector with the current values are shown in table 1

Table 1: Current known sources of detector uncertainties for liquid argon or TPC.

source of uncertainty	value	reference
e/ $\gamma$ separation		
e-m shower calibration		
hadronic shower calibration		
low energy acceptance electron identification		
.....		

Table 2: Current known sources of uncertainties due to interaction of charged particle with argon.

source of uncertainty	value	reference
pion(Kaon) absorbtion		
pion(Kaon) charge exchange		
pion (Kaon) production in secondary interactions		
muon capture	Phys. Rev. C 35, 2212	
energy scale		
Michel electron tagging		
.....		

<sup>137</sup> With current detector uncertainties from table 1 the sensitivities for the CP violation  
<sup>138</sup> phase measurement is shown in Fig. 2.1 **Task: make this plot**. The proposed test  
<sup>139</sup> beam detector will reduce uncertainties to XX% and improve our sensitivity to  $\delta_{CP}$  as  
<sup>140</sup> shown in Fig. 2.1 **Task: make this plot**.

Figure 1: Sensitivities for the  $\delta_{CP}$  measurement for using current knowledge of the single-phase LAr-TPC detector technology and for reduced detector uncertainties from SPCP beamtest data. The plots prepared for 40 kton fiducial mass and  $xx \times 10^{21}$ POT.

<sup>141</sup> **2.1.1 Particles energy and direction**

<sup>142</sup> Plans for running beam for the the ELBNF include both neutrino and anti-neutrino  
<sup>143</sup> configurations. These beams will be composed mainly of muon neutrinos (anti-neutrinos)  
<sup>144</sup> as well as electron neutrinos (anti-neutrinos). In figures 2.1.1 and 2.1.1 the distributions  
<sup>145</sup> on momenta and angles of particles created in neutrino interaction are shown.

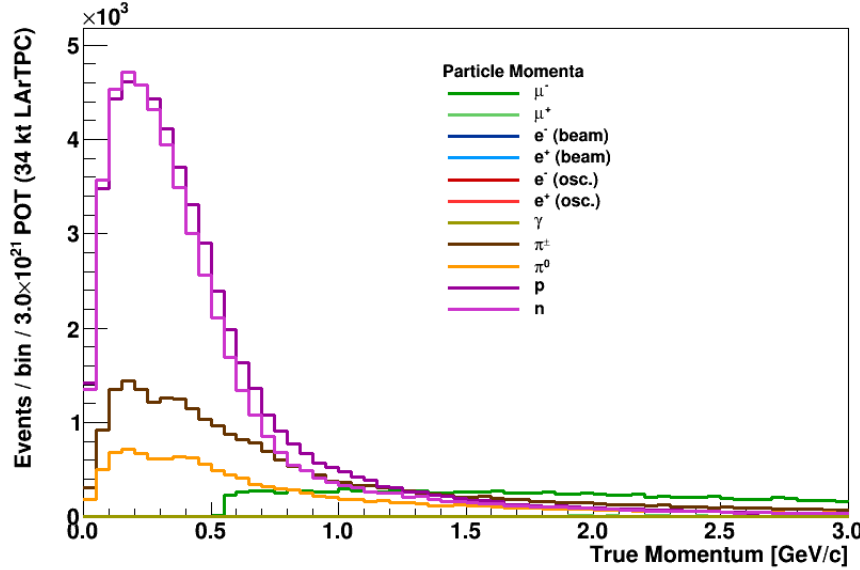


Figure 2: Particle momenta distributions for particles coming from all fluxes ( $\nu_e$ ,  $\nu_\mu$ ,  $\bar{\nu}_e$  and  $\bar{\nu}_\mu$ ) at both near and far detector locations.

Figure 3: Particle angle wrt to the beam axis distributions for particles coming from all fluxes ( $\nu_e$ ,  $\nu_\mu$ ,  $\bar{\nu}_e$  and  $\bar{\nu}_\mu$ ) at both near and far detector locations.

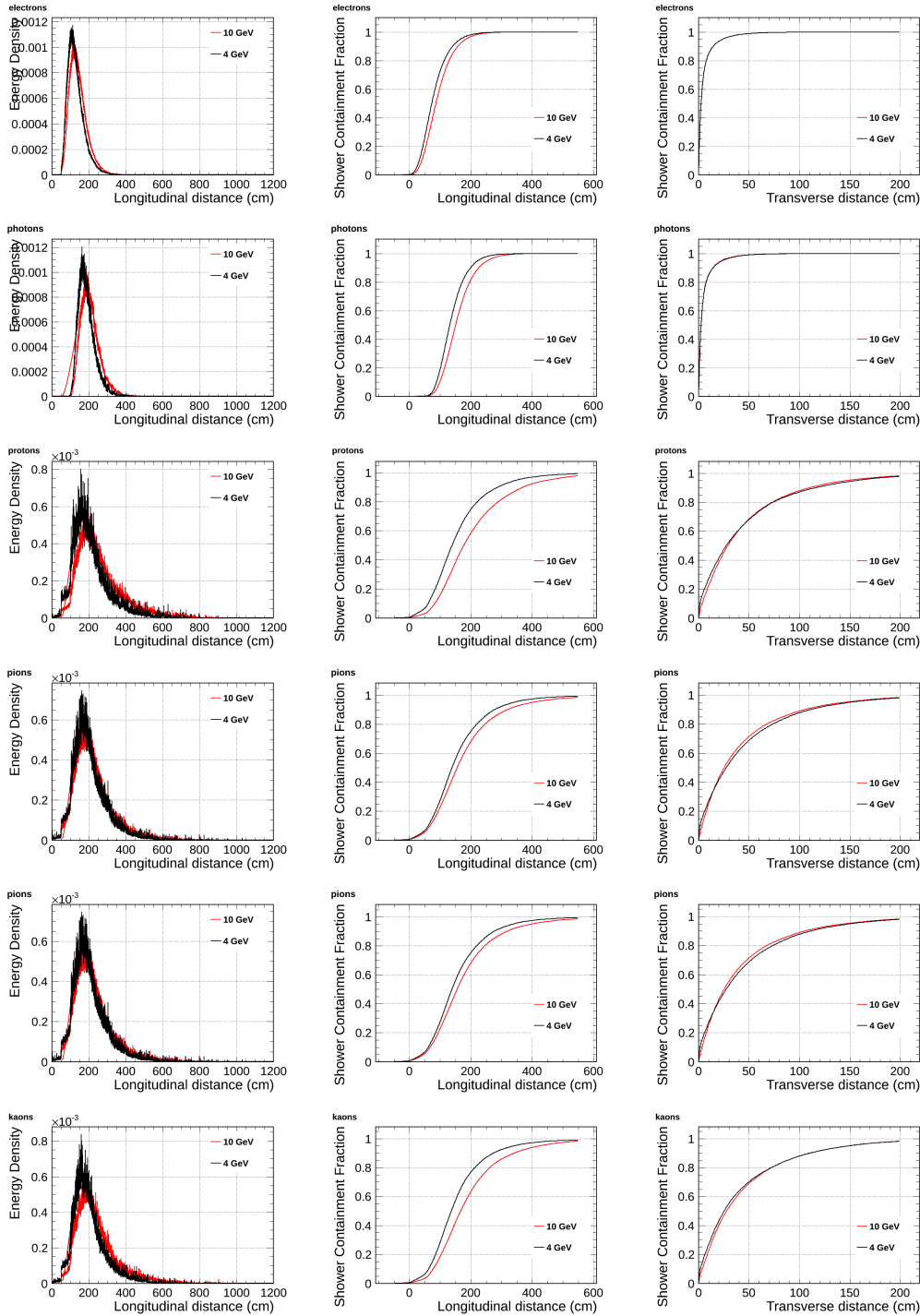


Figure 4: Particle containment plots.

<sup>146</sup> **2.1.2 Particle rates**

<sup>147</sup> Estimation of beam particles rates necessary to collect high enough statistics in a rea-  
<sup>148</sup> sonable time to obtain goals of the measurements.

<sup>149</sup> **2.1.3 Run plan**

<sup>150</sup> Based of the rates from the beam and required rates from the physics considerations.

<sup>151</sup> **2.2 Detector performance tests**

<sup>152</sup> **2.2.1 Bethe-Bloch parametrisation of charged particles**

<sup>153</sup> The SPCP will allow to study the detector response to charge particles from the test  
<sup>154</sup> beam and will serve as a calibration detector. The measured energy deposition for  
<sup>155</sup> various particles and its dependence on the direction of the particle will feed into our  
<sup>156</sup> Monte Carlo generator and allow more precise reconstruction of neutrino energy and  
<sup>157</sup> interactions topologies with good particle identifications.

<sup>158</sup> **How we compare with Lariat? Multiple scattering**

<sup>159</sup> The set of single-phase prototype detector helped to understand the detector response  
<sup>160</sup> to cosmic muons. But there is still lots to learn with additional studies. The charge  
<sup>161</sup> particle identification efficiencies has been mapped for only limited range of the particle  
<sup>162</sup> energies.

<sup>163</sup> **2.2.2 e/ $\gamma$  separation**

<sup>164</sup> The separation of the electrons from photons is the most important feature of the LAr  
<sup>165</sup> TPC detectors for the search of the CP violation phase where we look for appearance of  
<sup>166</sup> the  $\nu_e$  in the  $\nu_\mu$  beam. Showers from electrons are part of the signal whilst the single pho-  
<sup>167</sup> tons might contribute to the background sample. The photons can undergo two process:  
<sup>168</sup> pair production and Compton scattering. The dominant process for photons with ener-  
<sup>169</sup> gies of several hundreds MeV is the  $e^+ e^-$  pair production, but Compton scattering also  
<sup>170</sup> occur at this energies. For pair production the  $e/\gamma$  separation is achieved by looking at  
<sup>171</sup> the beginning of the electromagnetic shower, where for election we see energy deposition  
<sup>172</sup> typical for single MIP and for photon we see energy deposition consisted with two MIP.  
<sup>173</sup> The separation of  $e/\gamma$  has been measured in the ArgoNEUT experiment using neutrino  
<sup>174</sup> scattering data with low statistics. Currently the separation efficiency is estimated to be  
<sup>175</sup> at the level of of 94 % (? cite and check the number). In case of the Compton scattering  
<sup>176</sup> the off atomic electron the signal is much more difficult to distinguish from the electron  
<sup>177</sup> from the CC  $\nu_e$  scattering.

<sup>178</sup> The separation of the  $e/\gamma$  measured by ArgoNEUT is not sufficient for the ELBNF  
<sup>179</sup> experiment. Here we propose a measurement of the separation efficiency as the function  
<sup>180</sup> of energy and angle. **we need someone to look into this**

<sup>181</sup> **2.2.3 Reconstruction efficiencies and particle identification**

<sup>182</sup> The reconstruction of events in the LAr TPC is still a challenge but rapid progress has  
<sup>183</sup> been achieved in recent years (cite pandora and other reconstruction algorithms). De-

<sup>184</sup> spite the progress reconstruction algorithms have to rely Monte Carlo predictions which  
<sup>185</sup> don't simulate liquid argon detectors responses correctly. Reconstruction algorithms  
<sup>186</sup> will benefit greatly from test beam data particularly from the full scale prototype. The  
<sup>187</sup> reconstruction algorithms will be trained to correctly reconstruct track, electromagnetic  
<sup>188</sup> and hadronic showers.

<sup>189</sup> The data of tracks and showers can be used to create a library which can be used  
<sup>190</sup> for matching with he neutrino data, similar to the LEM (library event matching).

<sup>191</sup> Main issues for the reconstruction algorithms:

- <sup>192</sup> • The reconstruction algorithms try to use all three planes on the signal readout. if  
<sup>193</sup> the orientation of the track/shower is such that it is aligned with wires on one of  
<sup>194</sup> the plans it significantly reduces quality of reconstructed objects.
- <sup>195</sup> • Calorimetry with collection and induction planes. In the ICARUS experiment the  
<sup>196</sup> deposited energy was reconstructed from the signal on the collection plane. The  
<sup>197</sup> induction planes bipolar signal wasn't "stable" enough to use it for calorimetric  
<sup>198</sup> measurement. In the ELBNF design there is additional shielding wire plane which  
<sup>199</sup> will improve the quality of the bipolar signal and the test beam experiment will  
<sup>200</sup> help with its calibration.
- <sup>201</sup> • Vertexing.
- <sup>202</sup> • Reconstruction efficiency for low energy particles. The reconstruction algorithm  
<sup>203</sup> suffer from the lose of fefficiency for low energy particle or particles which leave  
<sup>204</sup> less than 200-300 hits. Training the algorithms on a low energy particles from the  
<sup>205</sup> test beam will improve the quality and efficiency of the reconstructed objects.

#### <sup>206</sup> 2.2.4 Cross section measurements

<sup>207</sup> Precise measurement of the absorption and charge exchange of pions and kaons. Pion  
<sup>208</sup> absorption is a large part of the pion nucleon cross section from 50 MeV to 500MeV with  
<sup>209</sup> no data above about 1GeV pion kinetic energy. **Add plots and values for known**  
<sup>210</sup> **cross sections wit errors**

- <sup>211</sup> • pion absorption on argon - Kotlinski, EPJ 9, 537 (2000)
- <sup>212</sup> • pion cross section as a function of A - Gianelli PRC 61, 054615 (2000)

<sup>213</sup> There is not currently a satisfactory theory describing absorption. The Valencia group  
<sup>214</sup> (Vicente-Vacus NPA 568, 855 (1994)) developed model of the pion-nucleus reaction with  
<sup>215</sup> fairly good agreement, although not in detail. The actual mechanism of multi-nucleon  
<sup>216</sup> absorption is not well understood.

#### <sup>217</sup> 2.2.5 Charge sign determination

<sup>218</sup> It is not possible to determine charge of the particle on the event by event basis with non-  
<sup>219</sup> magnetised LAr TPC detectors. However, the statistical analyst will be possible. We  
<sup>220</sup> will fit the muon's half time which is different for muons and antimony due to different  
<sup>221</sup> muon capture cross sections. For the  $\mu^+$  for argon we expect about xx% to be captured  
<sup>222</sup> and for  $\mu^-$  about yy%.

223 **2.2.6 Single track calibration**

224 **2.2.7 Shower calibration**

225 Reconstruction of neutrino energy depends of a quality of reconstruction of both elec-  
226 tromagnetic and hadronic showers.

227 - **features of Hadronic shower in LAr TPC - features of electromagnetic**  
228 **shower in LAr TPC - Missing energy from neutral (Neutrons scattering)**

229 **2.3 Other measurements**

230 **2.3.1 Anti-proton annihilation**

231 **2.3.2 Proton decay background (cosmogenic  $K^0 \rightarrow K^+$ )**

232 **3 Single Phase LAr Detector [ $\sim$ 10 pages; J. Stewart  
et al.]**

234 **3.1 LBNF detector**

235 The far detector for the ELBNF collaboration will be a series of four 17 kt (10 kt)  
236 a  (fiducial) volume liquid argon time projection chambers instrumented with photon  
237 detection. It is planned that the first 10 kt detector will be ready for installation in the  
238 2021 timeframe. One option for the TPC design is a wire plane based TPC with cold  
239 electronics readout. Designs of this style are referred to as single-phase detectors as  
240 the charge generation, drift, and detection all occurs in the argon liquid phase. This style  
241 TPC has the advantage that there is no charge amplification before collection making  
242 a very precise charge measurement possible. To achieve ELBNF's goals, a detector  
243 much larger than ICARUS, the largest LAr TPC detector built to date, is needed. The  
244 LBNE experiment was developing a scalable far detector design shown in Figure 5 that  
245 would scale-up LAr TPC technology by roughly a factor of 40 compared to the ICARUS  
246 T600 detector. To achieve this scale-up, a number of novel design elements need to  
247 be employed. A membrane cryostat typical for the liquefied natural gas industry will  
248 be used instead of a conventional evacuated cryostat. The wire planes or anode plane  
249 assemblies (APAs) will be factory-built as planar modules that are then installed into the  
250 cryostat. The modular nature of the APAs allow the size of the detector to be scaled up  
251 to at least 40 kt fiducial mass. Both the analog and digital electronics will be mounted  
252 on the wire planes inside the cryostat in order to reduce the electronic noise, to avoid  
253 transporting analog signals large distances, and to reduce the number of cables that  
254 penetrate the cryostat. The scintillation photon detectors will employ light collection  
255 paddles to reduce the required photo-cathode area. Many of the aspects of the design  
256 will be tested in a small scale prototype at Fermilab but given the very large scale of the  
257 detector elements a full-scale test is highly desirable. As the new ELBNF collaboration  
258 forms and organized a combined detector design team will emerge. Ideas from this new  
259 collaboration will modify the design presented here but this design provides a concrete  
260 example of a possible future detector.

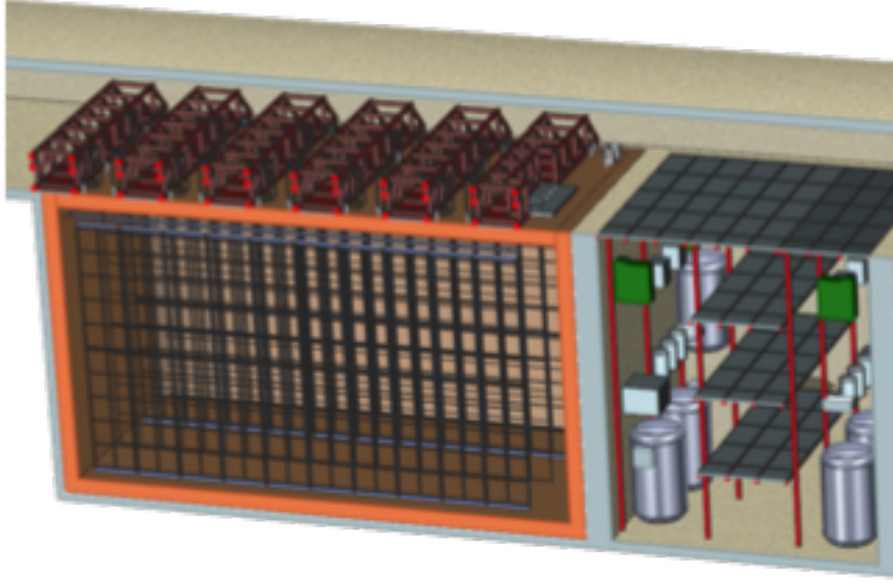


Figure 5: 3D model of one design of the ELBNF single-phase detector. Shown is 5kt fiducial volume detector which would need to be lengthened for the 10 kt design. The present ELBNF plan calls for the construction of 4 10 kt detectors of similar design.

261 The goals of the ELBNE detector test can be broken into four categories: argon  
 262 contamination mitigation verification, TPC mechanical verification, TPC electrical veri-  
 263 fication, and photon detection light yield verification. Research at Fermilab utilizing the  
 264 Materials Test Stand has shown that electronegative contamination to the ultra-pure  
 265 argon from all materials tested is negligible if the material is under the liquid argon.  
 266 This implies that the dominant source of contamination originates from the gas ullage  
 267 region and in the room temperature connections to the detector. Careful design of the  
 268 ullage region to insure that all surfaces and feedthroughs are cold is expected to greatly  
 269 reduce the sources of contamination over what exists in present detectors. Other con-  
 270 cepts attempt to eliminate the gas ullage completely. The goals related to mechanical  
 271 testing are to test the integrity of the detector. In the current design, each APA mea-  
 272 sures 2.3 m by 6.0 m and includes 2560 wires and associated readout channels. Given  
 273 the complexity of these assemblies, a test where the detector can be thermally cycled  
 274 and tested under operating conditions is highly advised prior to mass production. The  
 275 mechanical support of the APAs can be tested to verify that the mechanical design is  
 276 reliable and will accommodate any necessary motion between the large wire planes. The  
 277 impact of vibration isolation between the cryostat roof and the detector can also be  
 278 tested. Finally a potential improvement in the cryostat design is the possibility to move  
 279 the pumps external to the main cryostat. This will reduce any mechanical coupling to  
 280 the detector and also greatly improve both reliability and ease of repair. The electrical  
 281 testing goals are to insure that the high voltage design is robust and that the required  
 282 low electronic noise level can be achieved. As the detector scale increases so does the  
 283 capacitance and the stored energy in the device. The design of the field cage and high  
 284 voltage cathode planes needs to be such that HV discharge is unlikely and that if the  
 285 event occurs no damage to the detector or cryostat results. The grounding and shielding

286 of large detectors is also critical for low noise operation. By testing the full scale ele-  
287 ments one insures that the grounding plan is fully developed and effective. Large scale  
288 tests of the resulting design will verify the electrical model of the detector.

## 289 3.2 CERN prototype detector

### 290 3.2.1 Overview of the CERN Single-Phase test Detector

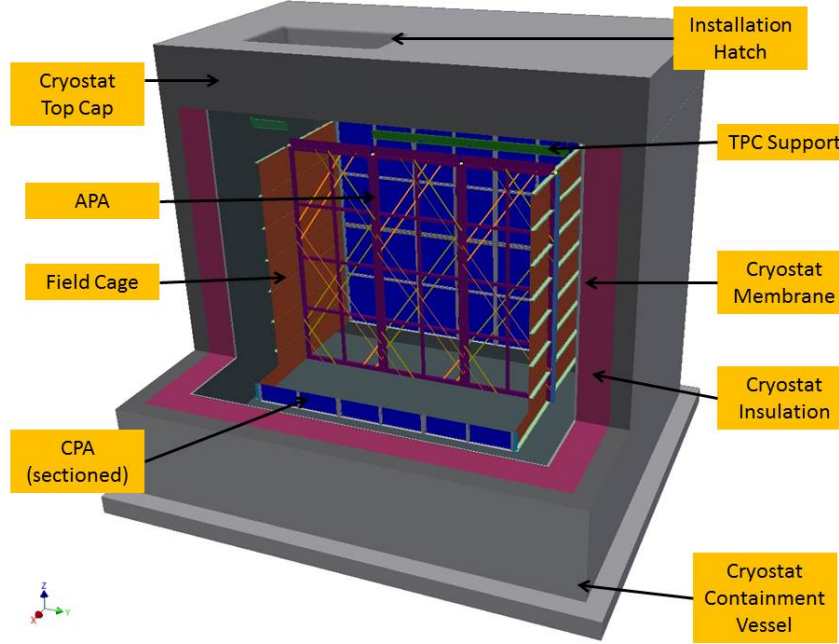


Figure 6: 3D model of the single-phase detector prototype is shown inside the test cryostat.

291 This sections presents the design details of a single-phase detector based on the  
292 development of the LBNE collaboration. As ELBNF moves forward the TPC working  
293 group will evaluate this and any modifications or alternate proposals. For the purpose  
294 of this proposal this represents one alternate, and it is expected to evolve as the new  
295 collaboration organized and more work is done.

296 This TPC consists of alternating anode plane assemblies (APAs) and cathode plane  
297 assemblies (CPAs), with field-cage panels enclosing the four open sides between the  
298 anode and cathode planes. Figure 6 shows a sectioned view for the planned TPC inside  
299 the cryostat at CERN. A uniform electric field is created in the volume between the anode  
300 and cathode planes. A charged particle traversing this volume leaves a trail of ionization.  
301 The electrons drift toward the anode plane, which is constructed from multiple layers of  
302 sense wires, inducing electric current signals in the front-end electronic circuits connected  
303 to the wires.

304 To the extent possible TPC will be assembled from elements that are of the same size  
305 as those planned for the single phase far detector. The primary exception to this is the  
306 length of the field cage panels which are 2.5m in this design, compared to 3.4m in the  
307 far detector. This is to reduce the impact of space charge on the prototype necessitated

308 by the surface operation. The overall size of the TPC will be derived by the size and  
309 number of anode planes (APA). It has been determined in order to perform the required  
310 physics, the TPC will consist of three APAs. The APAs will have an active (total) area  
311 2.29 m (2.32 m) wide and 6.0 m (6.2 m) high . The combination of the three APAs  
312 ~~will~~ determines the overall TPC length to be 7.2 m. There will be a cathode plane  
313 (CPA) on either side of the APAs. The overall width of the TPC will be determined  
314 by a combination of the drift distances along with the thickness of the APA, which is  
315 constructed of 3" x 4" stainless steel (SS) structural tubing. The overall width of the  
316 TPC is 5.2 m. Like the length of the TPC, the overall height will be determined by the  
317 height of the APA. The overall height of the TPC will be 6.3 m. In summary the external  
318 TPC dimensions will be 7.2 m long x 5.2 m wide x 6.3 m high. Along with the APAs  
319 and CPAs, the TPC will include a field cage that surrounds the entire assembly. It will  
320 be designed similarly to the field cage in phase 2 of the 35t experiment at FNAL. This  
321 is a series of pultruded fiberglass I beams for the structural elements. These I-beams  
322 will be tiled with large copper sided FR4 panels to create the field cage. Each panel will  
323 be connected with a series of resistors. The field cage will be connected to the CPAs  
324 through a capacitor assembly.

325 All of this will be supported by rows of I-beams supported from a mechanical struc-  
326 ture above the cryostat. The hangers for these I-beams will pass through the insulated  
327 top cap. There will be a series of feed thru flanges in the top cap of the cryostat to bring  
328 in and take out services for the TPC. There will be a HV feed thru for each of the CPAs  
329 and one signal feed thru for each of the APAs.

330 The minimum internal size of the cryostat is determined from size of the TPC. At the  
331 bottom of the cryostat there needs to be a minimum of 0.3 m between the frame of the  
332 CPA and closest point on the SS membrane. This is to prevent high voltage discharge  
333 between the CPA and the electrically grounded membrane. It is foreseen that there  
334 would be some cryogenic piping and instrumentation under the TPC. There is a height  
335 allowance of 0.1 m for this. There will be access and egress space around the outside of  
336 the TPC and the membrane walls. On three sides, 1.0 m of space is reserved for this.  
337 The final side of the TPC will have piping and instrumentation for the cryogenic system.  
338 There will be 1.3 m of space reserved for this.

339 The support system for the TPC will be located at the top between the underside  
340 of the cryostat roof and the top of the TPC. The plan is to model this space similar to  
341 what is planned for the far site TPC. There will be 0.9 m of ullage space. In order to  
342 prevent high voltage discharge, the upper most part of the CPA needs to be submerged a  
343 minimum of 0.3 m below the liquid Argon surface. The top of the TPC will be separated  
344 from the membrane by a minimum of 1.2 m.

345 Adding all of these to the size of the TPC yields the minimum inner dimensions of  
346 the cryostat. A minimally sized cryostat would be 9.5 m long, 7.3 m wide and 8.4 m  
347 high. This assumes the TPC will be positioned inside the cryostat with the CPAs and  
348 end field cages parallel to the walls of the cryostat. Also there is no space allotted for  
349 a beam window to enter the cryostat. Clearance would need to be added if it violates  
350 any of the current boundaries listed above.

351 These dimensions also preserve the ability to reverse the order of the APAs and  
352 CPAs inside the TPC. The current plan is to have the APAs located in the center of  
353 the cryostat with a CPA on each side. Reversing this to have the CPA in the center

354 and APAs on each side may be required to achieve some of the proposed physics. The  
 355 orientation of the TPC components will be finalized after various scenarios have been  
 356 sufficiently simulated.

357 **3.2.2 Anode Plane Assemblies (APAs)**

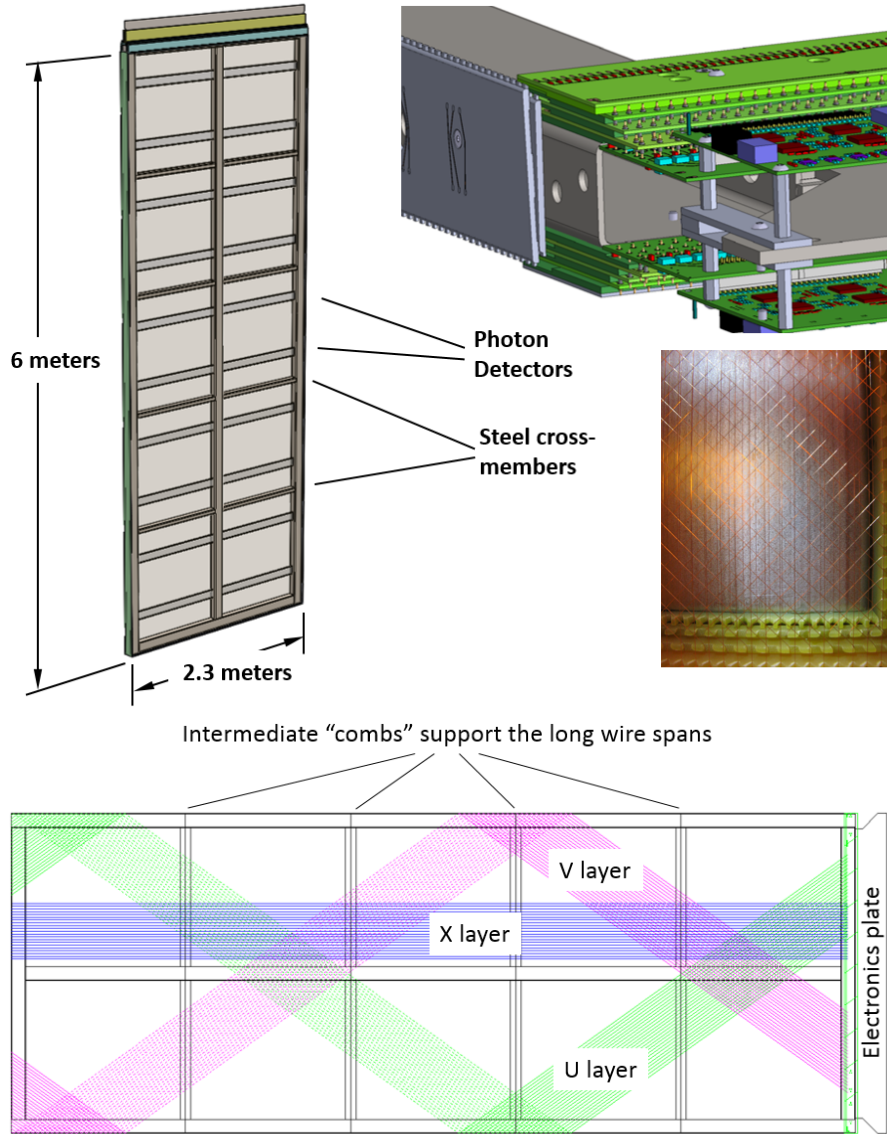


Figure 7: Clockwise from left: A full size APA, an APA corner showing the electronics boards, an APA lower corner photo showing wires and edge boards, and a figure showing the wire orientations and the placement of wire aligning combs.

358 Each APA (Figure 7) is instrumented with 3 layers of signal wires, one longitudinal  
 359 collection plane and two  $37.5^\circ$  angled induction planes with an additional outer grid plane  
 360 that helps maintain the field. The overall dimensions of the active area as mentioned  
 361 ~~able~~ are 2.3 m wide, 6 m long. The dimension of the wire planes were selected to fit down  
 362 the Ross shaft at SURF, be compatible with a standard HiCube transport container,

and allow construction from readily available materials. The angled layers start at the electronics end and wind around to the other side on their way to the bottom. The wire angle was selected so that a given angled induction wire will not overlay any longitudinal collection wire more than once in order to reduce ambiguities caused by the wrapped wire construction. Partial wire layers are shown here in Figure 7 at the bottom. With a wire pitches of 4.67 mm (diagonal layers) and 4.79 (straight layers), the total number of readout channels in an APA is 2560. The grid layer is not depicted in Figure 7 for clarity. The underlying structure of each APA is a framework of rectangular, stainless steel tubing. The side and bottom edges of the frame are lined with multiple layers of fiberglass circuit boards, notched along the edges to support and locate the wires that cross the APA face. A set of FR4 combs are glued to the APA frame to capture the wires at regular intervals. The front-end electronics boards are mounted at the top end of the frame and protected by a metal enclosure.

The distance between wire planes is 4.8 mm (3/16 in) corresponding with standard printed circuit board thickness, and while maintaining optimal signal formation. The four wire planes will be electrically biased so that electrons from an ionizing-particle track completely drift past the first three planes and are collected by the fourth plane. Calculations show that the minimum bias voltages needed to achieve this goal are  $V_G = -665V$ ,  $V_U = -370V$ ,  $V_V = 0V$  and  $V_X = 820V$  respectively (where G, U, V, and X are the wire-layer labels from outside in, towards the frame). It is convenient to set one of the wire planes to ground so that the wires can be DC coupled to the front-end readout electronics. In this instance, the V wire plane is set to ground potential to reduce the maximum bias voltages on the other wire planes, and enable the use of lower voltage rated AC coupling capacitors. A grounded mesh plane, located 4.8 mm behind the collection (X) plane, prevents the electric field around this set of wires from being distorted by the metal frame structure and the wires on the opposite side of the frame. It also shields the sensing wires from potential EM interferences from the photon detectors (Fig. 3.2.2) mounted within the frame. The mesh should have a wire pitch less than 2 mm to ensure a uniform electric field while maintaining a high optical transparency.

### 3.2.3 CPA and Field Cage

Each cathode plane (Fig. 9) is constructed from 6 identical CPA (cathode plane assembly) modules and two sets of end pieces. Each CPA is about half the size of an APA ( $2.3m \times 3.1m$ ) for ease of assembly and transport. The CPA is made of a stainless-steel framework, with 4 pieces of thin FR4 sheets mounted in the openings. A receptacle for the HV feedthrough is attached to the upper corner of a cathode plane toward the roof entrance side to mate with the HV feedthrough in the cryostat ceiling.

The FR4 sheets on the CPAs are treated with layers of high resistive coating on both sides. The resistivity of the coating will be chosen such that the surface potential does not deviate significantly with the ionization current from the cosmic rays, and forms a relatively long time constant to dissipate the stored energy on each sheet in case of a high voltage discharge. This long RC time constant will also reduce the peak current injected into the front-end electronics in a HV discharge.

Due to the relatively high cosmic ray flux in this surface detector, it is preferable to prevent the scintillation light emitted by a cosmic ray between the cathode and cryostat

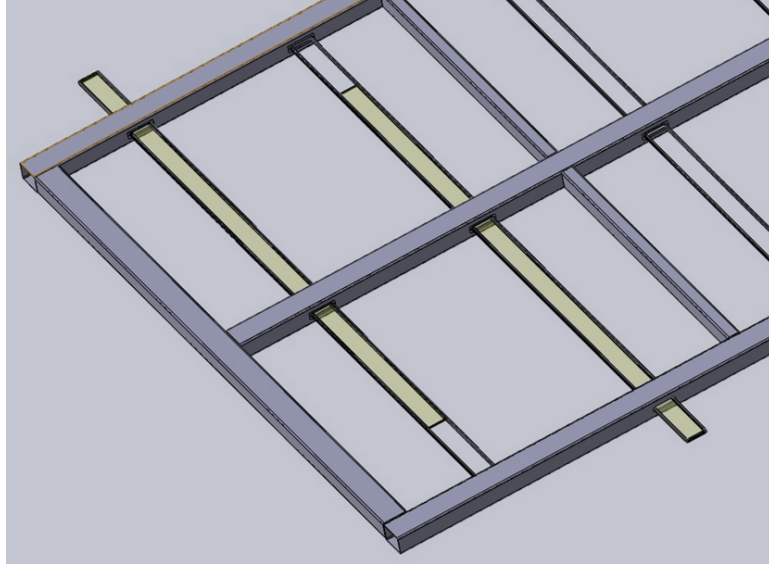


Figure 8: Photon detectors are mounted within the frame, between the wires on the two sets of four wire layers. The APA is built so that the photon detectors can be installed through slots in the side of the APA after the APA wires are installed. The wires that would cross these slots are routed around using copper traces on the edge boards.

407 wall from entering the TPC to reduce false trigger. The opaque cathode surface will  
 408 service this purpose. The high flux of cosmic rays combined with very low drift velocity  
 409 of positive ions in the liquid argon will result in sizable space charge distortions in  
 410 the TPC (docdb #6471). In addition, the positive ions could build up further if the  
 411 ion motion is slowed or stalled by counter flow in the LAr. Preliminary CFD analysis  
 412 (docdb #6140) have shown that solid cathodes in the cryostat result in LAr flow pattern  
 413 that neither causes excess positive ion buildup, nor degrades the LAr purity.

414 To achieve a 500 V/cm drift field over a 2.5 m distance, the bias voltage on the  
 415 cathode plane must reach  $-125$  kV. Two high voltage power supplies (150 – 200 kV) and  
 416 two HV feedthroughs will be needed for the two cathode planes. The HV feedthroughs  
 417 are based on the Icarus design, but modified to further improve the stability at higher  
 418 voltages.

419 Each pair of facing cathode and anode rows forms an electron-drift region. A field  
 420 cage completely surrounds the four open sides of this region to provide the necessary  
 421 boundary conditions to ensure a uniform electric field within, unaffected by the presence  
 422 of the cryostat walls.

423 The field cages are constructed using copper-clad FR4 sheets reinforced with fiber  
 424 glass I-beams to form panels of  $2.5\text{ m} \times 2.3\text{ m}$  in size for the top and bottom modules,  
 425 and  $2.5\text{ m} \times 2\text{ m}$  modules for the sides. Parallel copper strips are etched or machined  
 426 on the FR4 sheets. Strips are biased at appropriate voltages through a resistive divider  
 427 network. These strips will create a linear electric-potential gradient in the LAr, ensuring  
 428 a uniform drift field in the TPC’s active volume.

429 Since the field cage completely encloses the TPC drift region on four (of six) sides,  
 430 with the remaining two sides blocked by the solid cathodes, the FR4 sheets must be fre-  
 431 quently perforated to allow natural convection of the liquid argon. The “transparency”

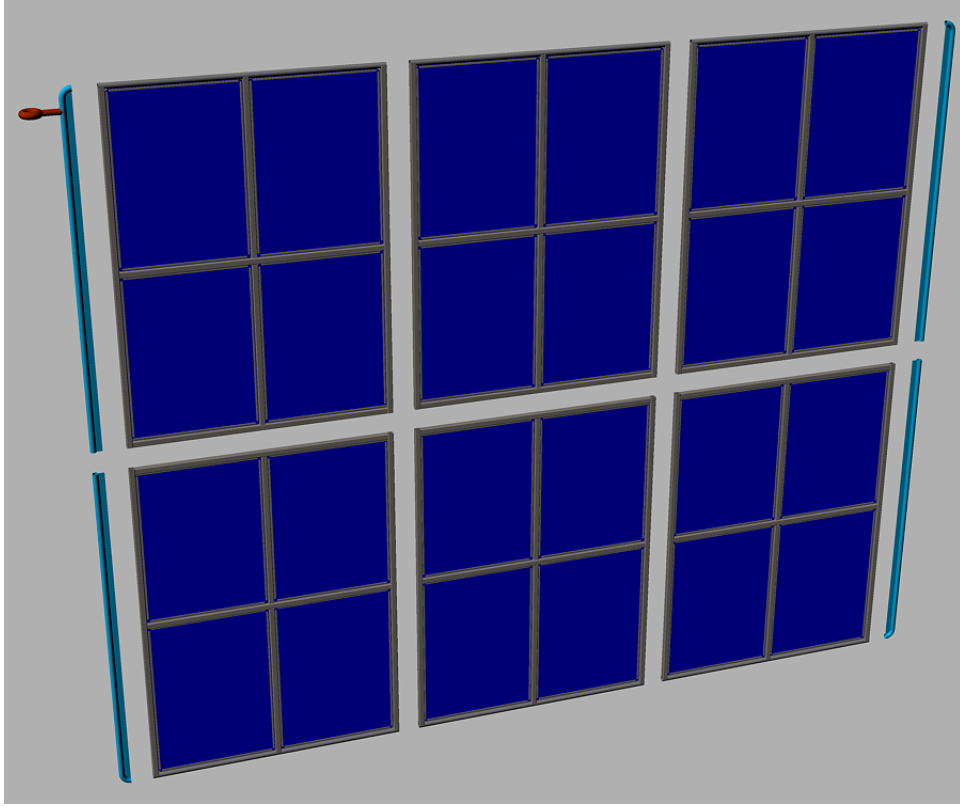


Figure 9: Exploded view of a cathode plane constructed from 6 CPA modules and 4 end pieces. The facing material on the CPA is highly resistive to minimize the peak energy transfer in case of a HV breakdown.

432 of the perforation will be determined by a detailed LAr computerized fluid dynamic  
 433 (CFD) study.

434 The left of Figure 10 shows a section of the field cage in the 35ton TPC as it was  
 435 being assembled. The 35ton TPC test results will inform us whether we should improve  
 436 upon the current design, or change the design concept all together for this and future  
 437 detectors. The main concern with the current field cage design is that the electric field  
 438 at the edges of the copper strips is still quite high due to the thinness of the copper.  
 439 One possible remedy is to cover the entire surface of the field cage with a high resistive  
 440 coating. The resistivity between strips due to this coating must be kept many orders  
 441 of magnitudes higher than the divider resistance to avoid distortion to the drift field.  
 442 Figure 10 (Right-Panel) shows an FEA simulation of such a configuration.

443 In the event of HV discharge on the cathode or the field cage, the voltage differential  
 444 between neighboring field cage strips near the discharge electrode will be very high  
 445 for a brief moment. This over voltage condition could cause damage to the field cage  
 446 electrode and the resistors installed between strips. To minimize such disk, varistors or  
 447 gas discharge tubes (GDT) will be installed between the field cage strips in parallel with  
 448 the resistors to prevent excess voltage transient between the electrodes.

449 In order to test the installation concept of the far detector, the top and bottom field  
 450 cage modules will be attached to the mating CPAs through hinges. These combined  
 451 assembly will be installed into the cryostat and the field cage module opens to bridge

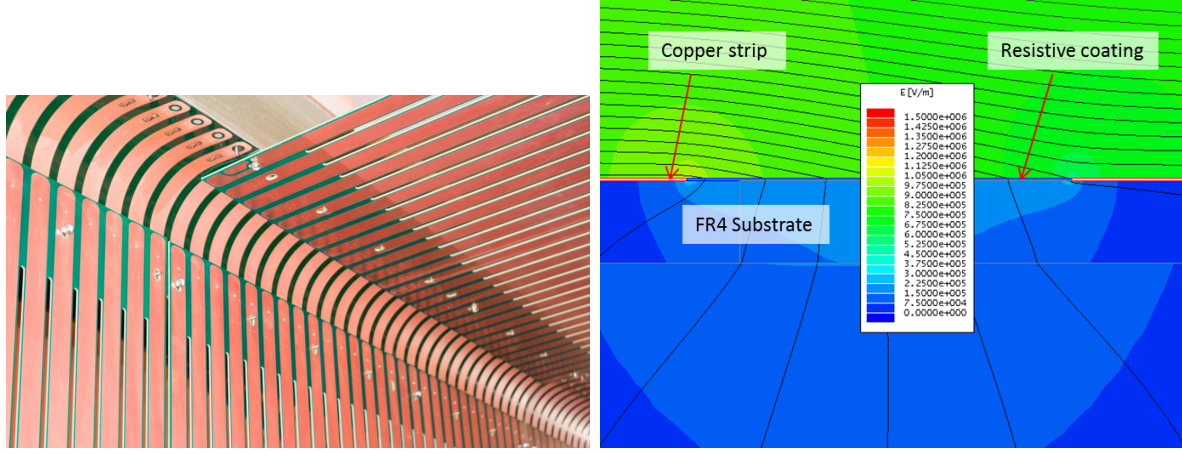


Figure 10: Left: A section of the field cage in the 35ton TPC. Right: Plot of electric field (color contours) and equi-potential contours (black lines) in a small region around the edges of two adjacent field cage strips on a 1.6mm thick FR4 substrate. A layer of resistive coating between the two copper strips nearly eliminated the high electric field regions at the copper edges

452 the CPA and the APA both mechanically and electrically.

453 **3.2.4 TPC Readout**

454 The electronics for the TPC is designed to operate at liquid argon temperature and is  
 455 places as close to the sense wires as possible. By minimizing the capacitance loading the  
 456 preamplifiers the electronics noise is greatly reduced. The present design has a maximum  
 457 wire length of 7.3 m (induction planes) with corresponding capacitance of 164 pF and  
 458 expected intrinsic noise of 400 electrons. In order to minimize any coupled noise and  
 459 to reduce the cable count a 12 bit cryogenic ADC operating at 2 MS/s has also been  
 460 designed which includes a 1:8 multiplexing stage. The output of the ADCs are then read  
 461 out by a commercial FPGA. The FPGA receives the data and is capable of providing  
 462 an additional factor of 4 in multiplexing if no zero suppression is applied. This data  
 463 is then sent out of the cryostat using the FPGAs high-speed (1 Gbps) serial links and  
 464 finally to the DAQ system. For the final detector it is expected that a dedicated digital  
 465 control and data transmission asic will be developed which replaces the commercial  
 466 FPGA but this work is only now starting and it will not be available at the start of  
 467 the CERN test. The front end electronics is organized as a stack of three boards: the  
 468 Analog Mother Board with the preamplifiers and ADCs that mounts on the APA, the  
 469 FPGA Mezzanine Board, and a SERDES Mezzanine Board serving as a cable interface.  
 470 Each analog mother board has eight preamplifiers/ADCs and instruments 128 wires. A  
 471 Faraday cage covers the end of the APAs to shield the electronics and also to prevent  
 472 any bubbles formed on the components from entering the active TPC volume. Figure  
 473 11 shows a schematic of the cold electronics.

474 Besides the high-speed signal cable, which is a twin-axial cable bundle manufactured  
 475 by GORE, there are cable bundles for low-voltage power, wire-bias voltages, and various  
 476 slow controls and monitoring. Redundant cables will be provided for many of these

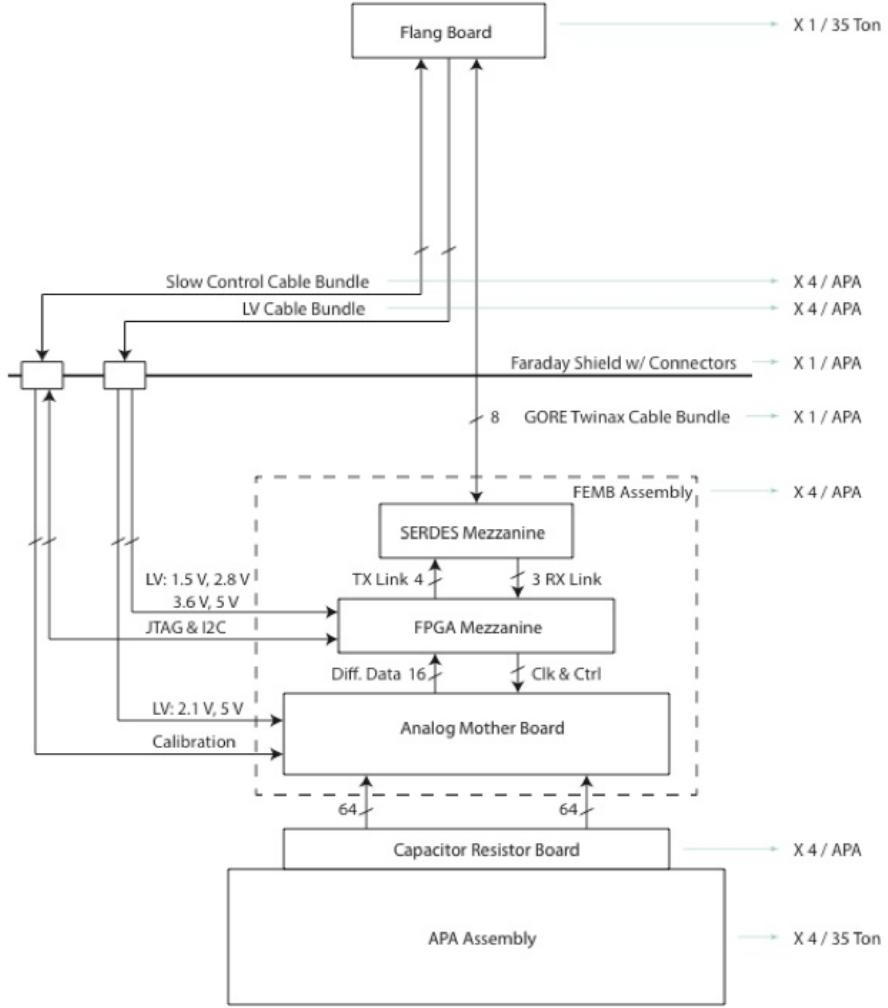


Figure 11: Layout of the TPC cold from end (FE) electronics..

477 functions. The cable bundles will be connected through a feedthrough on the roof of the  
 478 cryostat.

479 The primary interface between the TPC front-end electronics (FE) and the DAQ sub-  
 480 system consists of an ATCA-based system of RCEs (Reconfigurable Cluster Elements).  
 481 The RCE system receives the serialized raw data for the FE, performs zero-suppression  
 482 on it, and packetizes and transmits the resulting sparsified data to a back-end data farm  
 483 for event building and further processing. Additionally, the RCE system transmits tim-  
 484 ing and control signals to the FE as well as forwarding configuration data to them at  
 485 start-up.

486 The RCE system consists the following components: a commercial ATCA shelf (2-,  
 487 6-, or 14-slot), a Cluster-On-Board (COB) which is the "front board" in ATCA terms,  
 488 and a Rear-Transition-Module (RTM) which is the "rear board". A schematic of the  
 489 system is shown in Figure 12. The COB is a custom board, developed by SLAC, which  
 490 holds the processing power of the system. The COB (see Figure 12) consists of 5 bays for  
 491 holding daughter boards, an onboard 10-GbE switch, and both 10- and 1-Gb ethernet

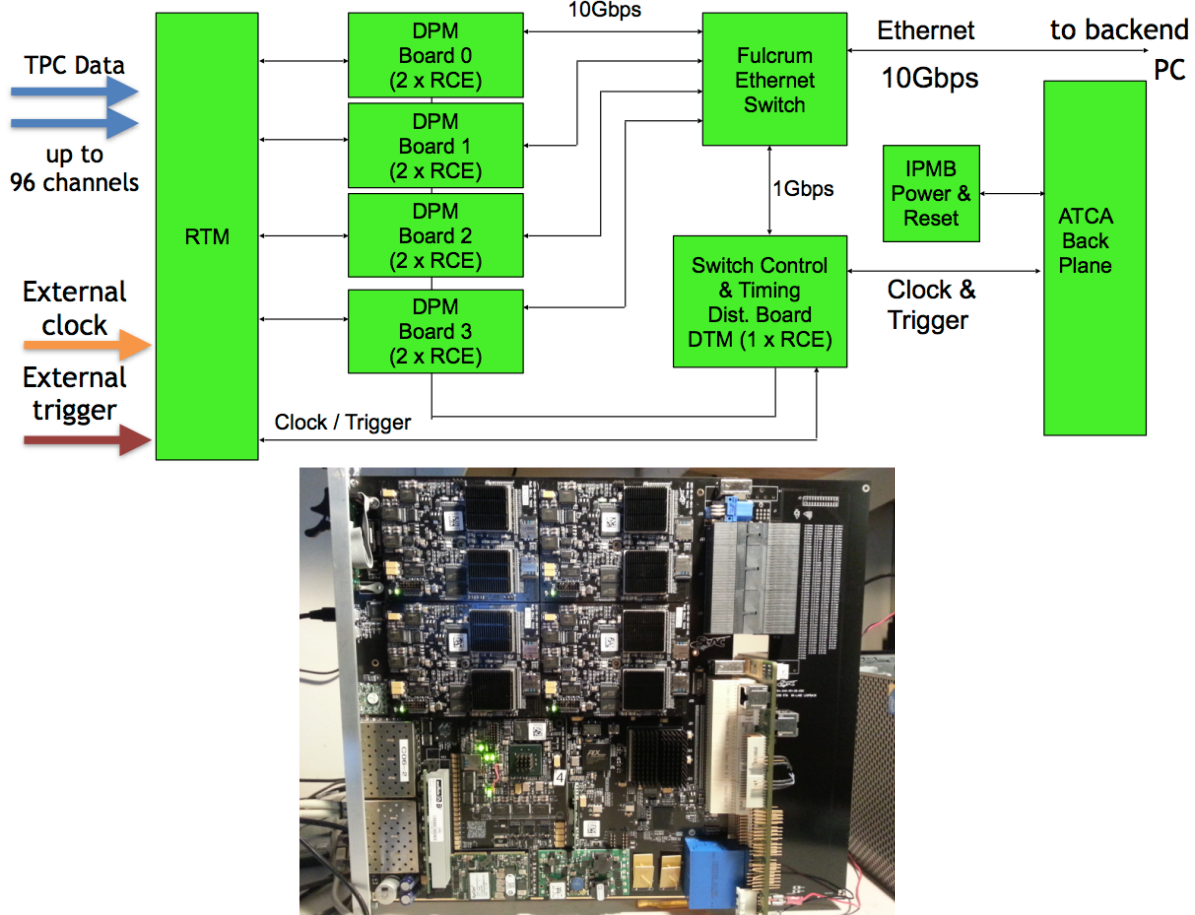


Figure 12: Top: Schematic for the TPC DAQ system. Bottom: The COB (left of the large connectors) and RTM (right).

492 connections for communications with the back-end system. Four of the daughter-board  
 493 bays are for Data Processing Modules (DPM), each of which can hold up to two RCEs.  
 494 The RCE is the core processing unit of the system; it is made up of a modern SoC  
 495 (currently, the Xilinx Zynq-7045) with multiple high-speed I/O ports (up to 10-Gbps  
 496 each) and external DRAM and flash memory controllers. The other bay on the COB  
 497 contains the Data Transmission Module (DTM) which is responsible for distributing  
 498 timing and trigger information to and between the DPMs.

499 While the COB hardware is application agnostic, the RTM is application specific.  
 500 The RTM provides the mechanical interface between the front-end (or, in our case, the  
 501 flange electronics) and the back-end, as well as other external sources such as the timing  
 502 or trigger systems. In this case we will use fiber optic connections between the flange  
 503 and the TPC DAQ using 8 12-channel (full duplex) CXP connectors on the RTM.

504 With the assumption that each cold FE board multiplexes its 128 wire channels to 4  
 505 outputs at 1-Gbps each, the non-zero suppressed data for 1 APA can be fed into a single  
 506 COB (containing 8 RCEs). Each RCE would receive data from 2 FE boards, perform  
 507 zero-suppression, and send the result to the back-end.

508 **3.2.5 Photon Detection System**

509 The ELBNF far detector will utilize liquid argon scintillation light to determine the  
510 prompt event time of beam-driven and non-beam events. While the TPC will have far  
511 superior spatial resolution to a photon detection system, the drift time for TPC events  
512 is on the order of milliseconds. The beam clock will give much better timing resolution  
513 than this but a photon detection system can determine the start of an event occurring  
514 in the TPC volume (or entering the volume) to about 6 ns, which will be useful in  
515 determining the  $t_0$  of cosmic ray events, events from radiological decays, and corrections  
516 to energy loss of the drifting electrons.

517 A charged particle passing through liquid argon will produce about 40,000 128 nm  
518 photons per MeV of deposited energy. At higher fields this will be reduced due to  
519 reduced recombination, but at 500 V/cm the yield is still about 20,000 photons per  
520 MeV. Roughly 1/3 of the photons are prompt 2-6 ns and 2/3 are generated with a  
521 delay of 1100-1600 ns. LAr is highly transparent to the 128 nm VUV photons with a  
522 Rayleigh scattering length and absorption length of 95 cm and >200 cm respectively.  
523 The relatively large light yield makes the scintillation process an excellent candidate for  
524 determination of  $t_0$  for non-beam related events. Detection of the scintillation light may  
525 also be helpful in background rejection.

526 Several prototypes of photon detection systems have been developed by the LBNE,  
527 now ELBNF, photon detector group over the past few years. There are currently three  
528 prototypes under consideration for use in the ELBNF far detector, a baseline design  
529 along with two alternate designs. A decision on the design to be deployed in the CERN  
530 test will be made in late 2015. The CERN neutrino platform ELBNF test would provide  
531 the first full scale test of the ELBNF photon detector fully integrated into a full scale  
532 TPC anode plane assembly.

533 The present reference design for the photon detection system is based on acrylic bars  
534 that are 200 cm long and 7.63 cm wide, which are coated with a layer of tetraphenyl-  
535 butadiene (TPB). The wavelength shifter converts VUV (128 nm) scintillation photons  
536 striking it to 430 nm photons inside the bar, with an efficiency of 50% of converting  
537 a VUV to an optical photon. A fraction of the wavelength-shifted optical photons are  
538 internally reflected to the bar's end where they are detected by SiPMs whose QE is well  
539 matched to the 430 nm wavelength-shifted photons. All PD prototypes are currently  
540 using SensL MicroFB-6K-35-SMT 6 mm ? 6 mm devices.

541 A full 6 m long APA will be divided into 5 bays with 2 PD modules (paddles)  
542 instrumenting each bay. The paddles will be inserted into the frames after the TPC  
543 wires have been wrapped around the frames allowing final assembly at the CERN test  
544 location. Two alternative designs are also under consideration.

545 One alternate design targeted increasing the geometrical acceptance of the photon de-  
546 tectors by using large acrylic TPB coated plates with imbedded WLS fibers for readout.  
547 In this design the number of required SiPMs and readout channels per unit detector area  
548 covered with photon detection panels would be significantly reduced to keep the overall  
549 cost for the photon detection system at or below the present design while increasing  
550 the geometrical acceptance at the same time. The prototype consists of a TPB-coated  
551 acrylic panel embedded with an S-shaped wavelength shifting (WLS) fiber. The fiber  
552 is read out by two SiPMs, which are coupled to either end of the fiber and serves to

553 transport the light over long distances with minimal attenuation. The double-ended  
554 fiber readout has the added benefit to provide some position dependence to the light  
555 generation along the panel by comparing relative signal sizes and arrival times in the  
556 two SiPMs.

557 The third design under consideration was motivated by increasing the attenuation  
558 length of the PD paddles and allowing collection of 400 nm photons coming from any-  
559 where in the active volume of the TPC. The fiber-bundle design is based on a thin TPB  
560 coated acrylic radiator located in front of a close packed array of WLS fibers. This  
561 concept is designed so that roughly half of the photons converted in the radiator are  
562 incident on the bundle of fibers, the wavelength shifting fibers are Y11 UV/blue with  
563 a 4% capture probability. The fibers are then read out using SiPMs at one end. The  
564 Y11 Kuraray fibers have mean absorption and emission wavelengths of about 440 nm  
565 and 480 nm respectively. The attenuation length of the Y11 fibers is given to be greater  
566 than 3.5 m at the mean emission wavelength, which will allow production of full-scale  
567 (2 m length) photon detector paddles.

568 The PD system tested at the CERN neutrino platform will be based on technology  
569 selected later this year. The technology selection process will be based on a series of  
570 tests planned for the next 6 months utilizing large research cryostats at Fermilab and  
571 Colorado State University. The primary metric used for comparison between the three  
572 technologies will be photon yield per unit cost. In addition to this metric PD threshold  
573 and reliability will also serve as inputs to the final decision. A technical panel will be  
574 assembled to make an unbiased decision.

575 Once the technology has been chosen the PD group will focus on optimizing the  
576 selected design with the goal of procurement and assembly taking place in late FY 2016  
577 and early FY 2016. The photon detector paddles will then be tested and shipped to  
578 CERN in early FY 2017 for installation into the APAs in late FY 2017 in preparation  
579 for installation into the test cryostat and operation in 2018.

### 580 3.2.6 DAQ, Slow control and monitoring

581 The DAQ will merge data to form events from the LArTPC, photon detector and beam  
582 detector readouts using the artDAQ data acquisition toolkit using a farm of commercial  
583 computers connected with an Ethernet switch. ArtDAQ is in use on several experiments  
584 at Fermilab. We are using it on the 35t prototype, so we will have considerable experience  
585 by the time of the CERN test.

586 The data collection for the CERN test will operate in a mode similar to that foreseen  
587 for the underground detectors. In order to collect data from non-beam interactions such  
588 as proton decay candidates or atmospheric neutrinos, data will be continuously read in  
589 to the artDAQ data receiver nodes and processed through the artDAQ system in quanta  
590 corresponding to time intervals fixed from the time of the beginning of the run. These  
591 are then transferred through the switch to a set of event building nodes which work in  
592 parallel, each node receiving all the data from all the detectors for the time intervals it  
593 is responsible for processing. There will be 32 parallel incoming data streams from the  
594 LArTPCs and 16 streams from the photon detectors. There will be an additional stream  
595 from the trigger board (the same board as built by Penn for the 35t test will be used)  
596 which will receive input of the spill gate, warning of extraction, and pattern-unit bits

597 from trigger counters and other beamline instrumentation such as Cerenkov counters  
598 [Which section are these described in?, should we refer to them from here?].

599 Synchronisation across all the input sources is essential in order that artDAQ can  
600 bring together the data from the input streams correctly for processing by the event  
601 building nodes. The data receiver nodes will provide overlap by repeating the data at  
602 the boundaries of the time intervals so that a particle whose data spans two time intervals  
603 can be collected. The time synchronisation is provided to the RTM back-module on the  
604 LArTPC readout crates, to the SSP photon detector readout and to the trigger board  
605 from a GPS based time synchronisation distribution system originally designed for the  
606 NOvA experiment. This system includes functionality to calibrate and correct for the  
607 cable delays, and to send synchronisation control signals to the readout at predetermined  
608 times.

609 The event building nodes will select time regions of interest within the time intervals  
610 they are processing and form these into events to be written to disk. The algorithms  
611 to select the events may be as simple as looking for a trigger bit in the trigger board  
612 data stream, or may involve looking for self-triggered events in the LArTPC data. An  
613 aggregation task, which is part of artDAQ will handle the parallelized event building  
614 processes by merging the output events into a single stream and writing them to disk. To  
615 avoid oversized output data files, when a predetermined file size is reached, the aggregator  
616 will switch to writing to a new file. The collaboration requests to CERN, data links of  
617 sufficient bandwidth to transfer these files from the CENF to the CERN data center,  
618 and from there to locations worldwide for analysis.

619 Improved versions of the software systems which are being prototyped at the 35t test  
620 will available for the CERN test including (a) Run control which controls and monitors  
621 the DAQ processes and allows run starts and stops to be performed by the operator  
622 (b) online monitoring (c) slow control of voltages and temperatures being used by the  
623 electronics (this may not be comprehensive by the time of the CERN prototype, but we  
624 plan on prototyping the readout of some of the quantities). The trigger board includes  
625 facilities for generating calibration pulses and for identifying the event times of the  
626 calibration events.

### 627 3.2.7 Installation

628 The interior of the cryostat will be prepared prior to the installation of the TPC. A series  
629 of support rails will be suspended below the top surface of the cryostat membrane. These  
630 will be structurally supported by a truss structure above the cryostat. These supports  
631 will pass through the top of the cryostat. They need to be designed to minimize the heat  
632 gain into the cryogenic volume. For the CPAs, the rails need to be electrically isolated  
633 due to high voltage concerns. To preserve the ability to reverse the order of the TPC  
634 components, all of the support rails will be designed to the same set of requirements  
635 regarding loads and attachment points.

636 There will be a series of feed thru flanges located along each of the support rails.  
637 These will be cryogenic flanges where the services for the TPC components can pass  
638 through the top of the cryostat. It is foreseen that each CPA will require one feed thru  
639 for the high voltage probe to bring in the drift voltage. The drift voltage is 500 V/cm.  
640 For a drift distance of 2.5 m, the probe voltage will be 125 kV. There will be one service

641 feed thru for each of the APAs. These feed thrus will include high speed data, bias  
642 voltages for the wire planes, control and power for the cold electronics.

643 The main TPC components will be installed through a large hatch in the top of the  
644 cryostat. This is similar to the installation method intended for the detector at the far  
645 site. This hatch will have an aperture approximately 2.0 m wide and 3.5 m long. Each  
646 APA and CPA panel will be carefully tested after transport into the clean area and  
647 before installation into one of the cryostats. Immediately after a panel is installed it will  
648 be rechecked. The serial installation of the APAs along the rails means that removing  
649 and replacing one of the early panels in the row after others are installed would be very  
650 costly in effort and time. Therefore, to minimize the risk of damage, as much work  
651 around already installed panels as possible will be completed before proceeding with  
652 further panels. The installation sequence is planned to proceed as follows:

- 653 1. Install the monorail or crane in the staging area outside the cryostat, near the  
654 equipment hatch.
- 655 2. Install the relay racks on the top of the cryostat and load with the DAQ and power  
656 supply crates.
- 657 3. Dress cables from the DAQ on the top of the cryostat to remote racks.
- 658 4. Construct the clean-room enclosure outside the cryostat hatch.
- 659 5. Install the raised-panel floor inside the cryostat.
- 660 6. Insert and assemble the stair tower and scaffolding in the cryostat.
- 661 7. Install the staging platform at the hatch entrance into the cryostat.
- 662 8. Install protection on (or remove) existing cryogenics instrumentation in the cryo-  
663 stat.
- 664 9. Install the cryostat feedthroughs and dress cables inside the cryostat along the  
665 support beams.
- 666 10. Install TPC panels:
  - 667 (a) Install both CPA panels. These will be installed from the floor of the cryostat.  
668 Access to the top edge will be required by scaffolding.
  - 669 (b) Install and connect HV probe for each of the CPAs.
  - 670 (c) Perform electrical tests on the connectivity of the probe to the CPAs.
  - 671 (d) Install first end wall of vertical field cage at the non-access end of the cryostat.  
672 These will be installed from the floor of the cryostat. Scaffolding will be  
673 needed to install the supporting structure and then attach the panels to the  
674 structure.
  - 675 (e) Test the inner connections of the field cage panels.
  - 676 (f) Install the first APA and connect to the far end field cage support.

- 677                             (g) Connect power and signal cables. This will require scaffolding to access the  
678                             top edge of the APA.
- 679                             (h) Test each APA wire for expected electronics noise. Spot-check electronics  
680                             noise while cryogenics equipment is operating.
- 681                             (i) Install the upper field cage panels for the first APA between the APA and  
682                             CPAs. This will require scaffolding to access the upper edge of the APA, CPA  
683                             and field cage structure.
- 684                             (j) Perform electrical tests on upper field cage panels.
- 685                             (k) Repeat steps (f) through (j) for the next two APAs.
- 686                             (l) Install the lower field cage panels between the APAs and CPAs. Start at the  
687                             far end away from the access hatch and work towards the hatch.
- 688                             (m) Perform electrical test on lower field cage panels and the entire loop around  
689                             the TPC.
- 690                             (n) Remove temporary floor sections as the TPC installation progresses.
- 691                             (o) Install sections of argon-distribution piping as the TPC installation pro-  
692                             gresses.
- 693                             (p) Install the final end wall of vertical field cage at the access end of the cryostat.  
694                             These will be installed from the floor of the cryostat. Scaffolding will be  
695                             needed to install the supporting structure and then attach the panels to the  
696                             structure.

- 697         11. Remove movable scaffold and stair towers.
- 698         12. Temporarily seal the cryostat and test all channels for expected electronics noise.
- 699         13. Seal the access hatch.
- 700         14. Perform final test of all channels for expected electronics noise.

701         In general, APA panels will be installed in order starting with the panel furthest  
702         from the hatch side of the cryostat and progressing back towards the hatch. The  upper  
703         field cage will be installed in stages as the installation of APA and CPAs progresses.  
704         After the APAs are attached to the support rods the electrical connections will be made  
705         to electrical cables that were already dressed to the support beams and electrical testing  
706         will begin. Periodic electrical testing will continue to assure that nothing gets damaged  
707         during the additional work around the installed APAs.

708         The TPC installation will be performed in three stages, each in a separate location;  
709         the locations, or zones. First, in the clean room vestibule, a crew will move the APA and  
710         CPA panels from storage racks, rotate to the vertical position and move them into the  
711         cryostat. Secondly, in the panel-staging area immediately below the equipment hatch of  
712         the cryostat, a second crew will transfer the lower panels from the crane to the staging  
713         platform, connect the upper and lower  panels together, route cables to the top of stacked  
714         panels and finally transfer the stacked panels on to the rails within the cryostat. A third  
715         crew will reposition the movable scaffolding and use the scaffold to make the mechanical

716 and electrical connections at the top for each APA and CPA as they are moved into  
717 position.

718 The requirements for alignment and survey of the TPC are under development. Since  
719 there will be plenty of cosmic rays in the surface detector and beam events, significant  
720 corrections can be made for any misalignment of the TPC. The current plan includes  
721 using a laser guide or optical transit and the adjustment features of the support rods  
722 for the TPC to align the top edges of the APAs in the TPC to be straight, level and  
723 parallel within a few mm. The alignment of the TPC in other dimensions will depend  
724 on the internal connecting features of the TPC. The timing of the survey will depend  
725 on understanding when during the installation process the hanging TPC elements are  
726 in a dimensionally stable state. The required accuracy of the survey is not expected to  
727 be finer than a few mm.

## 728 4 Cryostat and cryogenics system [~5 pages; **David/Barry/Jack**

729 Describe requirements to meet detector goals

### 730 4.1 LBNF detector

731 This section to provide context and illustrate which aspects need testing at the CERN  
732 prototype

733 (Probably can take text from CDR once it's more developed)

### 734 4.2 CERN prototype detector

#### 735 4.2.1 Cryostat from David Montanari

736 The Single Phase TPC test at CERN will use a membrane tank technology to contain  
737 the base design of 725 tons of LAr equivalent to about  $520m^3$ . The design is based on  
738 a scaled up version of the LBNE 35 Ton Prototype and the Fermilab Short Baseline  
739 Near Detector. We propose that the cryostat be housed in the extension of the EHN1  
740 Bat 887 at CERN, where the cryogenic system components will also be located. The  
741 cryostat will use a steel outer supporting structure with a metal liner inside to isolate  
742 the insulation volume, similar to the one of the dual phase detector prototype WA105  
743  $1 \times 1 \times 3$  and to the Fermilab Short Baseline Near Detector. The support structure  
744 will rest on I-beams to allow for air circulation underneath to maintain the temperature  
745 within the allowable limits. The scope of the EHN1 cryostat subsystem includes the  
746 design, procurement, fabrication, testing, delivery and oversight of a cryostat to contain  
747 the liquid argon and the TPC. This section describes a reference design, whose scope  
748 encompasses the following components:

- 749 • steel outer supporting structure,
- 750 • main body of the membrane cryostat (sides and floor),
- 751 • top cap of the membrane cryostat.

752 A membrane cryostat design commonly used for liquefied natural gas (LNG) storage  
753 and transportation will be used. In this vessel a stainless steel membrane contains  
754 the liquid cryogen. The pressure loading of the liquid cryogen is transmitted through  
755 rigid foam insulation to the surrounding outer support structure, which provides external  
756 support. The membrane is corrugated to provide strain relief resulting from temperature  
757 related expansion and contraction. The vessel is completed with a top cap that uses the  
758 same technology.

759 Two membrane cryostat vendors are known: GTT (Gaztransport & Technigaz) from  
760 France and IHI (Ishikawajima-Harima Heavy Industries) from Japan. Each one is tech-  
761 nically capable of delivering a membrane cryostat that meets the design requirements  
762 for this detector. To provide clarity, only one vendor is represented in this document,  
763 GTT; this is for informational purposes only. Figure 1 shows a 3D model of the GTT  
764 membrane and insulation design.

765 The conceptual reference design for the Single Phase Test at CERN cryostat is a  
766 rectangular vessel measuring 9.5 m in length (parallel to the beam direction), 7.3 m in  
767 width, and 8.40 m in height; containing a total mass of 725 tons of liquid argon. Figure 15  
768 shows side and end views of the cryostat respectively. Figure 3 shows a 3D view. To  
769 minimize the contamination from warm surfaces, during operation the temperature of  
770 all surfaces in the ullage shall be lower than 100 K. The top plate will contain two  
771 hatches to install the TPCs and enter the tank, a manhole and several penetrations for  
772 the cryogenic system and the detector.

### 773 **Design Parameters (from David Montanari)**

774 This design is meant to test technical solutions that may be of interest for future  
775 needs of the Long Baseline Neutrino program. The use of a cold ullage (<100 K) to lower  
776 the impurities in the gas region, and of a LAr pump outside the cryostat to minimize  
777 the effect of noise, vibration and microphonics to the TPC inside the LAr are Value  
778 Engineering studies for the Long Baseline program.

779 The design parameters for the TPC Test at CERN cryostat are listed in Table 3.

### 780 **Insulation system and secondary membrane (from David Montanari)**

781 The membrane cryostat requires insulation applied to all internal surfaces of the  
782 outer support structure and roof in order to control the heat ingress and hence required  
783 refrigeration heat load. The maximum ~~required~~ static heat leak is  $15W/m^2$  for the floor  
784 and the sides and  $20W/m^2$  for the roof. Preliminary calculations show that it can be  
785 obtained using 0.8 m thick insulation panels. Given an average thermal conductivity  
786 coefficient for the insulation material of  $0.0283 W/(m\cdot K)$ , the heat input from the sur-  
787 rounding steel is expected to be about 3.7 kW total. It assumes that the hatches are  
788 foam insulated as well. This is shown in Table 4.

789 The insulation material is a solid reinforced polyurethane foam manufactured as  
790 composite panels. The panels get laid out in a grid with 3 cm gaps between them  
791 (that will be filled with fiberglass) and fixed onto anchor bolts anchored to the support  
792 structure. The composite panels contain the two layers of insulation with the secondary  
793 barrier in between. After positioning adjacent composite panels and filling the 3 cm  
794 gap, the secondary membrane is spliced together by epoxying an additional overlapping  
795 layer of secondary membrane over the joint. All seams are covered so that the secondary  
796 membrane is a continuous liner.

# GST® Containment System

## AS A PRIMARY BARRIER :

### a flexible (1.2mm) stainless steel membrane



The double network of corrugations absorbs the thermal contractions due to the very low temperature of the LNG.

## Insulating panel

The thickness of the panels can be adjusted to provide a large range of boil-off rates according to the operator's requirements (typically 0.05% per day).

## Plywood

## Reinforced polyurethane foam

## AS A SECONDARY BARRIER :

### a composite laminated material

This consists of a thin sheet of aluminium between two layers of glass cloth and resin.

In the event of a failure of the primary membrane, it prevents the build-up of stress concentrations on concrete corner and ensures the liquid tightness of the concrete wall.

## Reinforced polyurethane foam

## Plywood

## Mastic

## Post-tensionned concrete covered by a moisture barrier

The outer concrete container provides the *structural resistance* to internal (LNG hydrostatic & dynamic pressure, and vapour gas pressure) and external (wind, snow, ice) loads.

A moisture barrier, applied on its inner side, prevents moisture from entering the tank.

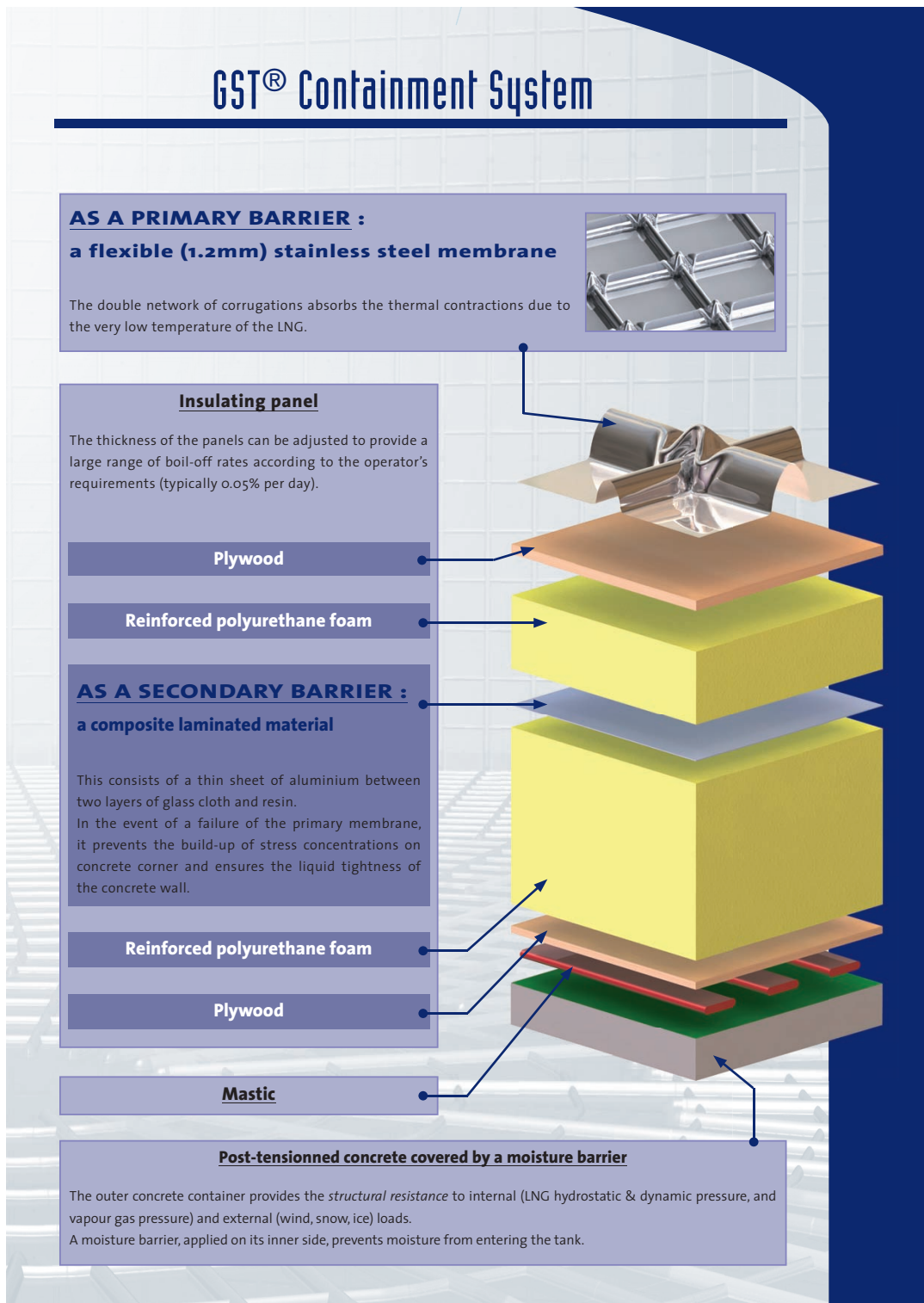


Figure 13: Exploded view of the membrane cryostat technology

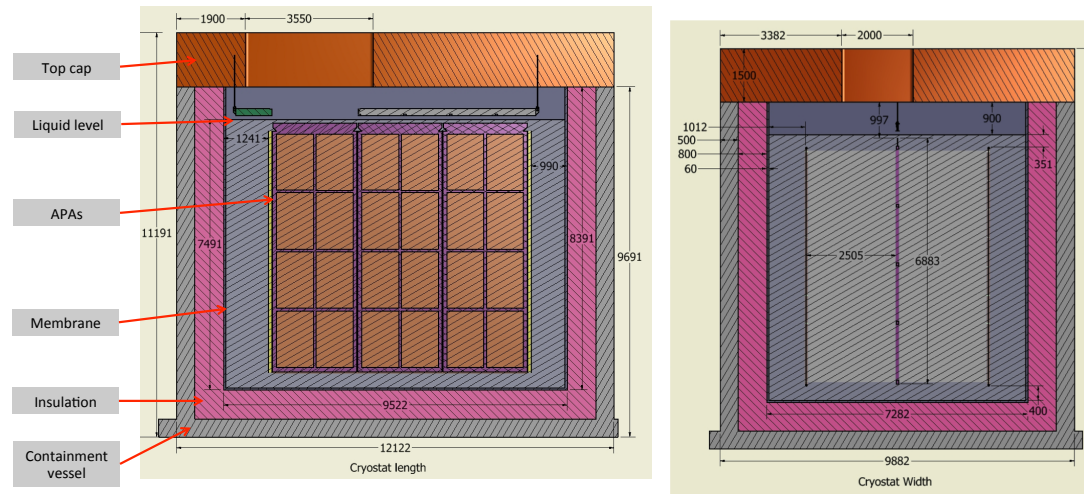


Figure 14: Side (left) and end (right) views of cryostat

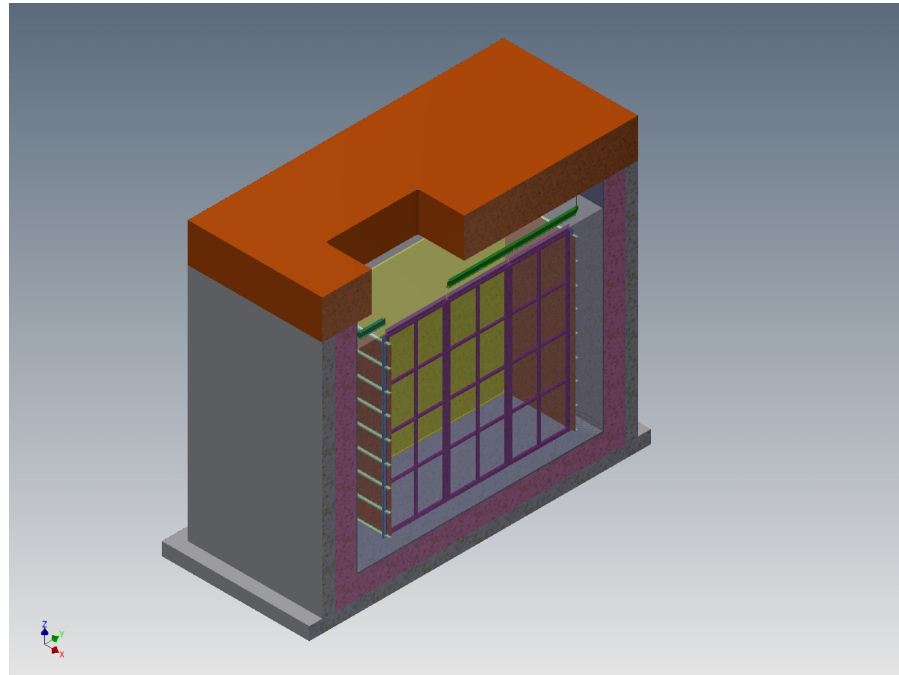


Figure 15: Isometric view of the membrane cryostat

Table 3: Design requirements for the cryogenic system (has right values)

Design Parameter	Value
Type of structure	Membrane cryostat
Membrane material	SS 304/304L, 316/316L or equivalent. Other materials upon approval.
Outside reinforcement (support structure)	Steel enclosure with metal liner to isolate the outside from the insulation space, standing on legs to allow for air circulation underneath.
Total cryostat volume	583 m3
Total LAr volume	520 m3
LAr total mass	725,000 kg
Minimum inner dimensions (flat plate to flat plate).	7.3 m (W) x 9.5 m (L) x 8.4 m (H)
Depth of LAr	7.5 m (0.9 m ullage, same as LBNF)
Primary membrane	1.2 mm thick SS 304L corrugated stainless steel
Secondary barrier system	0.07 mm thick aluminum between fiberglass cloth. Overall thickness 1 mm located between insulation layers.
Insulation	Polyurethane foam (0.8 m thick from preliminary calculations)
Maximum static heat leak	15 W/m2 
LAr temperature	88 +/- 1K
Operating gas pressure	Positive pressure. Nominally 70 mbarg ( 1 psig)
Vaccum	No vacuum
Design pressure	350 mbarg ( 5 psig) + LAr head (1,025 mbarg)
Design temperature	77 K (liquid nitrogen temperature for flexibility)
Temperature of all surfaces in the ullage during operation	
Leak tightness	<100 
Maximum noise/vibration/microphonics inside the cryostat	LAr pump outside the cryostat
Beam window	In the center of the active volume. Precise location TBD.
Accessibility after operations	Capability to empty the cryostat in 30 days and access it in 60 days after the end of operations.
Lifetime / Thermal cycles	Consistent with liquid argon program. TBD.

797 The secondary membrane is comprised of a thin aluminum sheet and fiberglass cloth.  
 798 The fiberglass- aluminum-fiberglass composite is very durable and flexible with an overall  
 799 thickness of about 1 mm. The secondary membrane is placed within the insulation space.  
 800 It surrounds the bottom and sides. In the unlikely event of an internal leak from the  
 801 primary membrane of the cryostat into the insulation space, it will prevent the liquid  
 802 cryogen from migrating all the way through to the steel support structure where it would  
 803 degrade the insulation thermal performance and could possibly cause excessive thermal  
 804 stress in the support structure. The liquid cryogen, in case of leakage through the inner  
 805 (primary) membrane will escape to the insulation volume, which is purged with GAr at  
 806 the rate of one volume exchange per day.

Table 4: Heat load calculation for the membrane cryostat (insulation thickness = 0.8 m). (note to self: has right values)

Element	Area ( $m^2$ )	K (W/mK)	$\Delta T$ (K)	Heat Input (W)
Base	83	0.0283	205	605
End walls	190	0.0283	205	1,374
Side walls	149	0.0283	205	1,081
Roof	83	0.0283	205	605
Total				3,665

### 807 Cryostat Configuration (from David Montanari)

808 This section describes the configuration of the cryostat only. The TPC is described  
 809 in Section xxx. With the intent to minimize the contamination in the gas region, the  
 810 ullage will be kept cold (<100 K). A possible way to achieve this requirement is to spray  
 811 a mist of clean liquid and gaseous argon to the metal surfaces in the ullage and keep  
 812 them cold, similar to the strategy that was developed for the cool down of the LBNE 35  
 813 Ton prototype.

### 814 Outer Support Structure (from David Montanari)

815 The reference design is a steel support structure with a metal liner on the inside  
 816 to isolate the insulation region and keep the moisture out. This choice allows natural  
 817 and forced ventilation to maintain the temperature of the steel within acceptable limits,  
 818 without the need of heating elements and temperature sensors. It reduces the time  
 819 needed for the construction: the structure will be prefabricated in pieces of dimensions  
 820 appropriate for transportation, shipped to the destination and only assembled in place.  
 821 Fabrication will take place at the vendor's facility for the most part. This shortens the  
 822 construction of the outer structure on the detector site, leaving more time for completion  
 823 of the building infrastructure. If properly designed, a steel structure may allow the  
 824 cryostat to be moved, should that be desired later in the future.

### 825 Main body of the membrane cryostat (from David Montanari)

826 The sides and bottom of the vessel constitute the main body of the membrane cryo-  
 827 stat. They consist of several layers. From the inside to the outside the layers are stainless  
 828 steel primary membrane, insulation, thin aluminum secondary membrane, more insula-  
 829 tion, and steel outer support structure with meal panels acting as vapor barier. The

secondary membrane contains the LAr in case of any primary membrane leaks and the vapor barrier prevents water ingress into the insulation. The main body does not have side openings for construction. The access is only from the top. There is a side penetration for the liquid argon pump for the purification of the cryogen.

#### **Top cap (from David Montanari)**

Several steel reinforced plates welded together constitute the top cap. The stainless steel primary membrane, intermediate insulation layers and vapor barrier continue across the top of the detector, providing a leak tight seal. The secondary barrier is not used nor required at the top. The cryostat roof is a removable steel truss structure that bridges the detector. Stiffened steel plates are welded to the underside of the truss to form a flat vapor barrier surface onto which the roof insulation attaches directly. The penetrations will be clustered in the back region, as far away from the beam as possible. The top cap will have a large opening for TPC installation, a secondary smaller opening for personnel access and a manhole.

The truss structure rests on the top of the supporting structure where a positive structural connection between the two is made to resist the upward force caused by the slightly pressurized argon in the ullage space. The hydrostatic load of the LAr in the cryostat is carried by the floor and the sidewalls. Everything else within the cryostat (TPC planes, electronics, sensors, cryogenic and gas plumbing connections) is supported by the steel plates under the truss structure. All piping and electrical penetration into the interior of the cryostat are made through this top plate, primarily in the region of the penetrations to minimize the potential for leaks. Studs are welded to the underside of the top plate to bolt the insulation panels. Insulation plugs are inserted into the bolt-access holes after panels are mounted. The primary membrane panels are first tack-welded then fully welded to complete the inner cryostat volume.

Table 5 presents the list of the design parameters for the top of the cryostat.

#### **Cryostat grounding and isolation requirements (from David Montanari)**

The cryostat has to be grounded and electrically isolated from the building. This section presents the list of the current grounding and isolation requirements for the cryostat. Figure 16 shows the layout of the top plate grounding.

#### **Isolation**

1. The cryostat membrane and any supporting structure, whether it is a steel structure or a concrete and rebar pour, shall be isolated from any building metal or building rebar with a DC impedance greater than  $300\text{ k}\Omega$ .
2. All conductive piping penetrations through the cryostat shall have dielectric breaks prior to entering the cryostat and the top plate.

#### **Grounding**

1. The cryostat, or “detector” ground, shall be separated from the “building” ground.
2. A safety ground network consisting of saturated inductors shall be used between detector ground and building ground.
3. Parameters TBD.

#### **Top plate grounding**

Table 5: Design parameters for the cryostat top (has right values)

<b>Design Parameter</b>	<b>Value</b>
Configuration	Removable metal plate reinforced with trusses anchored to the membrane cryostat support structure. Contains multiple penetrations of various sizes and a manhole. Number, location and size of the penetrations TBD. Provisions shall be made to allow for removal and re-welding six (6) times.
Plate/Trusses non-wet material	Steel if room temperature. SS 304/304 or equivalent if at cryogenic temperature
Wet material	SS 304/304L, 316/316L or equivalent. Other materials upon approval.
Fluid	Liquid argon (LAr)
Design pressure	350 mbarg ( 5 psig)
Design temperature	77 K (liquid nitrogen temperature for flexibility)
Inner dimensions	To match the cryostat
Maximum allowable roof deflection	0.028 m (span/360 from LBNF)
Maximum static heat leak	<20 W/m <sup>2</sup>
Temperatures of all surfaces in the ullage during operation	<100 K
Additional design loads	<ul style="list-style-type: none"> <li>- Top self-weight</li> <li>- TPC ( 3,000 kg on each anchor)</li> <li>- TPC anchors (TBD)</li> <li>- Live load (488 kg/m<sup>2</sup>)</li> <li>- Electronics racks (400 kg in the vicinity of the feed through)</li> <li>- Services (150 kg on every feed through)</li> </ul>
TPC anchors	Capacity: 3,000 kg each anchor. Number and location TBD. Minimum 6.
Hatch opening for TPC installation	3,550 m x 2,000 m (location TBD)
Grounding plate	1.6 mm thick copper sheet brazed to the bottom of the top plate
Lifting fixtures	Appropriate for positioning the top at the different parts that constitute it.
Cold penetrations	Minimum 4 (??). Location and design TBD.
Lifetime / Thermal cycles	Consistent with the liquid argon program TBD.

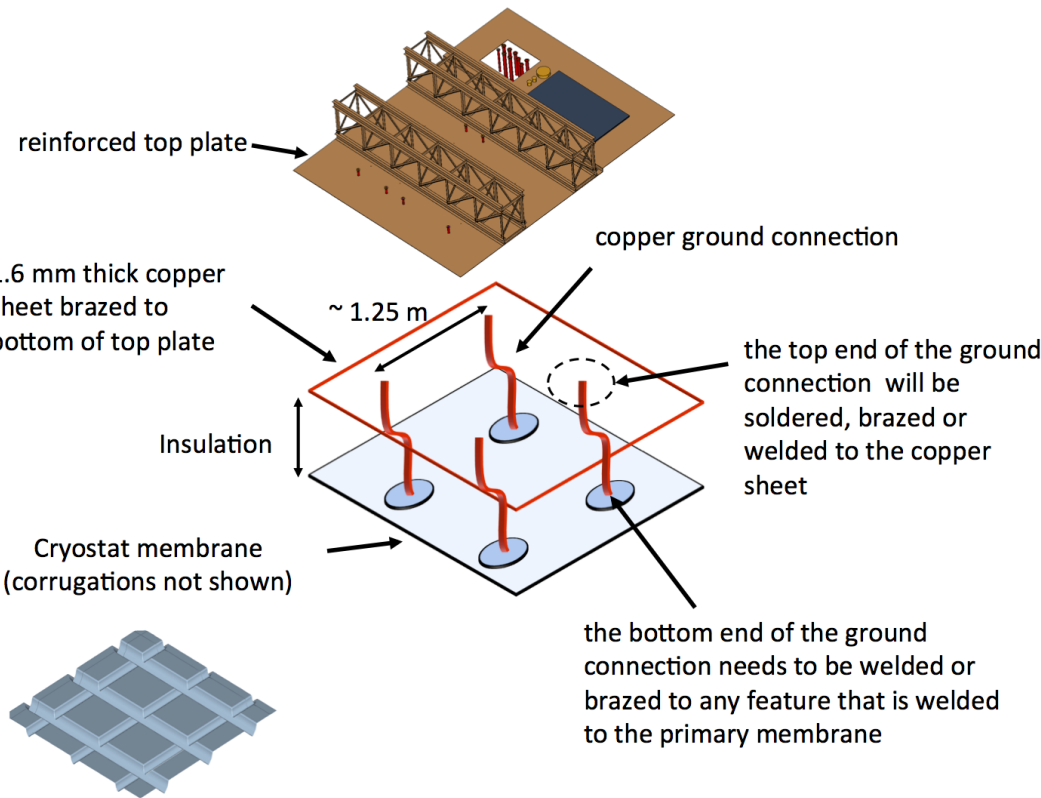


Figure 16: Top plate grounding layout

- 872 1. If the cryostat is contained within a concrete pour, the top plate shall be electrically  
873 connected to any rebar used in that pour, and the rebar shall be conductively tied  
874 at regular intervals. Parameters TBD.
- 875 2. The top grounding plate shall be electrically connected to the cryostat membrane  
876 by means of copper braid connections.
  - 877 (a) Each connection shall be at least 1.6 mm thick and 63.5 mm wide.
  - 878 (b) The length of each connection is required to be as short as possible.
  - 879 (c) The distance between one connection and the next one shall be no more than  
880 1.25 m.
  - 881 (d) The layout can follow the profile of several pieces of insulation, but it shall  
882 be continuous.
  - 883 (e) The DC impedance of the membrane to the top plate shall be less than 1  
884 ohm.

#### 885 **Leak prevention (from David Montanari)**

886 The primary membrane will be subjected to several leak tests and weld remediation,  
887 as necessary. All (100%) of the welds will be tested by an Ammonia colorimetric leak  
888 test (ASTM E1066-95) in which welds are painted with a reactive yellow paint before

889 injecting a Nitrogen-Ammonia mixture into the insulation space of the tank. Wherever  
890 the paint turns purple or blue, a leak is present. The developer is removed, the weld  
891 fixed and the test is performed another time. Any and all leaks will be repaired. The  
892 test lasts a minimum of 20 hours and is sensitive enough to detect defects down to  
893 0.003 mm in size and to a  $10^{-7} \text{ std } - \text{cm}^3/\text{s}$  leak rate (equivalent leak rate at standard  
894 pressure and temperature, 1 bar and 273 K). To prevent infiltration of water vapor  
895 or oxygen through microscopic membrane leaks (below detection level) the insulation  
896 spaces will be continuously purged with gaseous argon to provide one volume exchange  
897 per day. The insulation space will be maintained at 30 mbar, slightly above atmospheric  
898 pressure. This space will be monitored for changes that might indicate a leak from the  
899 primary membrane. Pressure control devices and safety relief valves will be installed on  
900 the insulation space to ensure that the pressure does not exceed the operating pressure  
901 inside the tank. The purge gas will be recirculated by a blower, purified, and reused as  
902 purge gas. The purge system is not safety- critical; an outage of the purge blower would  
903 have negligible impact on LAr purity.

#### 904 **Cryostat size from TPC dimensions (from Jack Fowler)**

905 The minimum internal size of the cryostat is determined from size of the TPC. At the  
906 bottom of the cryostat there needs to be a minimum of 0.3 m between the frame of the  
907 CPA and closest point on the SS membrane. This is to prevent high voltage discharge  
908 between the CPA and the electrically grounded membrane. It is foreseen that there  
909 would be some cryogenic piping and instrumentation under the TPC. There is a height  
910 allowance of 0.1 m for this. There will be access and egress space around the outside of  
911 the TPC and the membrane walls. On three sides, 1.0 m of space is reserved for this.  
912 The final side of the TPC will have piping and instrumentation for the cryogenic system.  
913 There will be 1.3 m of space reserved for this.

914 The support system for the TPC will be located at the top between the underside  
915 of the cryostat roof and the top of the TPC. The plan is to model this space similar to  
916 what is planned for the far site TPC. There will be 0.9 m of ullage space. In order to  
917 prevent high voltage discharge, the upper most part of the CPA needs to be submerged a  
918 minimum of 0.3 m below the liquid Argon surface. The top of the TPC will be separated  
919 from the membrane by a minimum of 1.2 m.

920 Adding all of these to the size of the TPC yields the minimum inner dimensions of  
921 the cryostat. A minimally sized cryostat would be 9.5 m long, 7.3 m wide and 8.4 m  
922 high. This assumes the TPC will be positioned inside the cryostat with the CPAs and  
923 end field cages parallel to the walls of the cryostat. Also there is no space allotted for  
924 a beam window to enter the cryostat. Clearance would need to be added if it violates  
925 any of the current boundaries listed above. These dimensions also preserve the ability  
926 to reverse the order of the APAs and CPAs inside the TPC. The current plan is to have  
927 the APAs located in the center of the cryostat with a CPA on each side. Reversing this  
928 to have the CPA in the center and APAs on each side may be required to achieve some  
929 of the proposed physics. The orientation of the TPC components will be finalized after  
930 various scenarios have been sufficiently simulated.

931 **4.3 Cryogenic System (from David Montanari)**

932 The cryogenic system is being developed as part of the international engineering team  
933 set up between Fermilab and CERN to design, fabricate and install cryogenic systems  
934 of similar requirements and increased size for Short and Long Baseline at Fermilab, and  
935 WA105s at CERN. The goal is to develop a single model and adapt if for all future  
936 generation detectors, with the necessary scaling up in size and adjustments for eventual  
937 different needs of the different detectors. Table 6 presents the list of requirements for  
938 the cryogenic system for the Single Phase TPC test at CERN detector.

939 Figure 17 outlines the basic scheme of the LN2 supply system, which was proposed  
940 by CERN for the Short Baseline Program and agreed as an appropriate solution for  
941 this detector as well. The experiment will rely on LN2 tankers for regular deliveries to a  
942 local dewar storage, which will be sized to provide several days of cooling capacity in the  
943 event of a delivery interruption. From the dewar storage the LN2 is then transferred to a  
944 distribution facility located in the experimental hall. It includes a small buffer volume  
945 and an LN2 pumping station that transfers the LN2 to the argon condenser and other  
946 services as needed. The low estimated heat leak of the vessel ( 3.5 kW) and the location  
947 inside an above ground building allow for use of an open loop system typical of other  
948 installations operated at Fermilab (LAPD, LBNE 35 ton prototype, MicroBooNE) and  
949 at CERN (???). Main goal of the LN2 system is to provide cooling power for the argon  
950 condenser, the initial cool down of the vessel and the detector, and all other services as  
951 needed.

952 Figure 18 shows a schematic diagram of the proposed liquid argon system. It is based  
953 on the design of the LBNE 35 ton prototype, the MicroBooNE detector systems and the  
954 current plans for the Long Baseline Far Detector.

955 Main goal of the LAr system is to purge the tank prior to the start of the operations  
956 (with GAr in open and closed loop), cool down the tank and fill it with LAr. Then con-  
957 tinuously purify the LAr and the boil off GAr to maintain the required purity (electron  
958 lifetime measured by the detector).

959 The LAr receiving facility includes a storage dewar and an ambient vaporizer do  
960 deliver LAr and GAr to the cryostat. The LAr goes through the liquid argon handling  
961 and purification system, whereas the Gar through the gaseous argon purification before  
962 entering the vessel. The LAr purification system is currently equipped with a filter  
963 containing mol sieve and copper beds, and a regeneration loop to regenerate the filter  
964 itself. The filter medium may change following the ongoing developments on filtration  
965 schemes, but the concept remains the same.

966 During operation, an external LAr pump circulates the bulk of the cryogen through  
967 the LAr purification system. The boil off gas is first re-condensed and then is sent to  
968 the LAr purification system before re- entering the vessel.

Table 6: Design requirements for the cryogenic system

Parameter	Value
Location	Preferably not in front of the cryostat (on the beam)
Cooling Power	TBD based on the heat leak of the cryostat (estimated 3.5 kW), the cryo-piping and all other contributions (cryogenic pumps, etc.)
Liquid argon purity in cryostat	10 ms electron lifetime (30 ppt O <sub>2</sub> equivalent)
Gaseous argon piston purge rate of rise	1.2 m/hr
Membrane cool-down rate	From manufacturer
TPCs cool-down rate	<40 K/hr, <10 K/m (vertically)
Mechanical load on TPC	The LAr or the gas pressure shall not apply a mechanical load to the TPC greater than 200 Pascal.
Nominal LAr purification flow rate (filling/ops)	5.5 day/volume change
Temperature of all surfaces in the ullage during operations	<100 K
Gaseous argon purge within insulation	1 volume change /day of the open space between insulation panels.
Lifetime of the cryogenic system	Consistent with the LAr program. TBD.

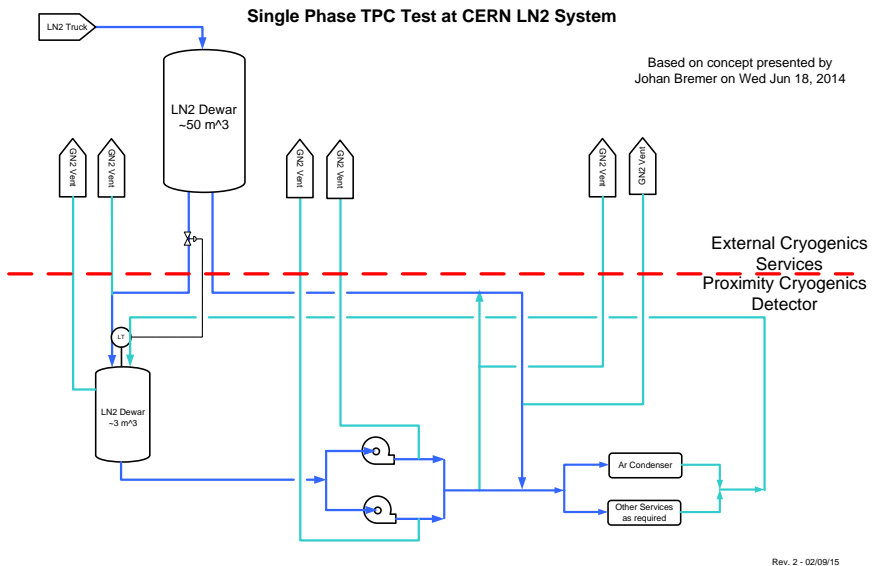


Figure 17: Schematic diagram for the proposed LN2 system

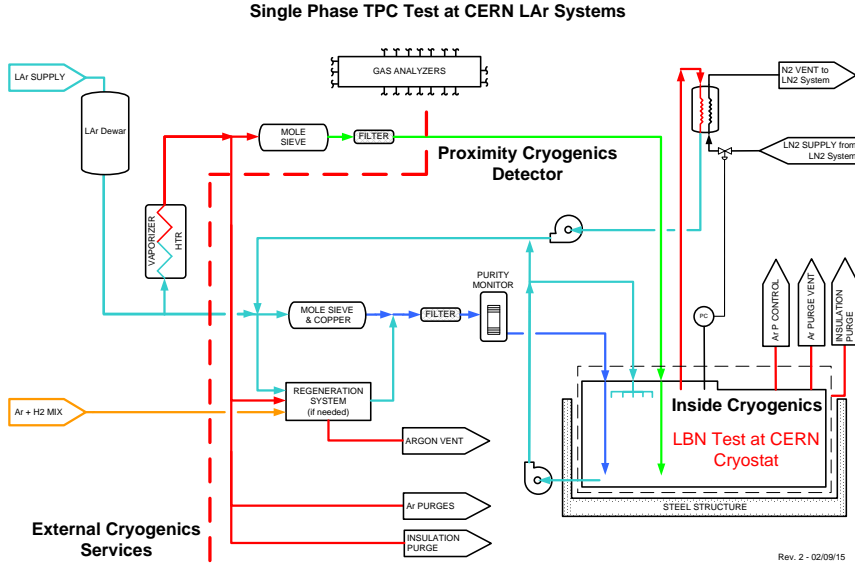


Figure 18: Schematic diagram for the proposed LAr system

## 969 5 Charged Particle Test Beam Requirements [ $\sim 10$ 970 pages; Cheng-Ju]

### 971 5.1 Particle Beam Requirements

972 The requested beam parameters are driven by the requirement that the results from the  
 973 CERN test beam should be directly applicable to the future large underground single-  
 974 phase LAr detector with minimal extrapolation. The CERN test beam data will be  
 975 used to evaluate the detector performance, to understand the various physics systematic  
 976 effects, and to provide “neutrino-like” data for event reconstruction studies. The chosen  
 977 beam parameters span a broad range of particle spectrum that are expected in the future  
 978 neutrino experiment. The particle beam composition should consist of electrons, muons,  
 979 and hadron beams that are charge-selected. The particle momentum of interest ranges  
 980 from 0.2 GeV/c to 10 GeV/c. The maximum electron drift time in the TPC is about  
 981 3 ms. To minimize pile-up in the TPC, the desired beam rate should be around 200  
 982 Hz with the maximum rate below 300 Hz. The single-phase TPC consists of two drift  
 983 volumes. It is desirable to aim the particle beam so that hadronic showers are mostly  
 984 contained in the same drift volume. However, we also plan to take some data with  
 985 hadronic shower crossing the midplane of the TPC from one drift volume to another.  
 986 The two beam entry angles and positions with respect to the LAr cryostat are illustrated  
 987 in Figure [XYZ.] The summary of the beam requirements are shown in Table 7.

### 988 5.2 EHN1 H4ext Beamline

989 The H4ext is an extension of the existing H4 beamline in Experimental Hall North 1  
 990 (EHN1). To produce particles in the momentum range of interest, 60 - 80 GeV/c pion  
 991 beam from the T2 target is used to generate tertiary beams. The tertiary particles are

Table 7: Particle beam requirements.

Parameter	Requirements	Notes
Particle Types	$e^\pm, \mu^\pm, \pi^\pm$	
Momentum Range	0.2 - 10 GeV/c	
Momentum Spread	$\Delta p/p < 5\%$	
Transverse Beam Size	RMS(x,y) < 2.5 cm	At the entrance face of the LAr cryostat
Beam Divergence		
Beam Angle	$\approx 20^\circ$	
Beam Dip Angle	-6° (nominal); $\pm 5^\circ$ range	
Beam Entrance Position		
Rates	200 Hz (average); 300 Hz (maximum)	

<sup>992</sup> momentum and charge-selected and transported down H4ext beamline to the experimental area. A preliminary layout of the H4ext beamline is shown in Figure 19.

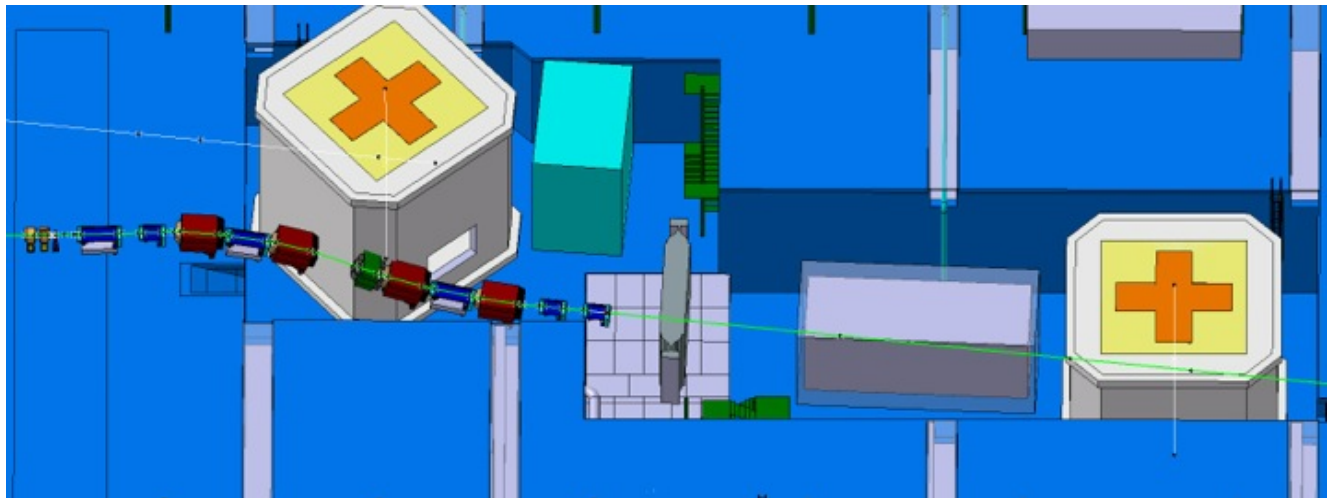


Figure 19: Preliminary layout of the H4ext beamline

### <sup>994</sup> 5.2.1 Beam Optics

<sup>995</sup> [Waiting for inputs from Ilias]

### <sup>996</sup> 5.2.2 Expected Rates and Purity

<sup>997</sup> [Waiting for inputs from Ilias]

998 **5.3 Beam Instrumentation**

999 **5.3.1 Beam Position Detector**

1000 **5.3.2 Time-of-Flight Detector**

1001 **5.3.3 Threshold Cherenkov Counter**

1002 **5.4 Muon Beam Halo Counters**

1003 The halo counter is a set of plastic scintillator paddles surrounding the beamline. The  
1004 main purpose is to tag particles (primarily muons from the upstream production target)  
1005 that are outside of the beam axis, but may potentially enter the TPC volume. The  
1006 counter information is used to either veto or simply flag these class of events.

1007 **5.5 Beam Window on LAr Cryostat**

1008 This section could be absorbed into the cryostat chapter.

1009 **6 Computing requirements, data handling and soft-  
1010 ware [~3 pages; Maxim Potekhin/Craig Tull ]**

1011 **6.1 Overview**

1012 The proposed “Full Scale” test of a single-phase Liquid Argon TPC at CERN will build  
1013 upon the technology and expertise developed in the process of design and operation of  
1014 its smaller predecessor, the 35t detector at FNAL. This includes elements of front-end  
1015 electronics, data acquisition, run controls and related systems. We also expect that for  
1016 the most part, Monte Carlo studies necessary to support this program will be conducted  
1017 utilizing software evolved from tools currently used (2015).

1018 In the test-beam setup, the detector performance will be characterized for different  
1019 types of particles, e.g.  $p$ ,  $\pi^\pm$ ,  $\mu^\pm$  etc (see 2.1). Current plans call for measurements  
1020 in pre-defined bins of the incident particle momentum, which will have widths ranging  
1021 from tens to hunderds of MeV (see 6.2.3). The volume of data to be recorded shall be  
1022 determined by the number of events that need to be collected in each measurements  
1023 that is provides adequately low statistical uncertainty of the parameters measured.

1024 In our view, it is optimal to first stage the “precious” data collected from the proto-  
1025 type on disk at CERN and then sink it to tape (also at CERN), while simultaneously  
1026 performing replication to data centers in the US. For the latter, FNAL is the prime  
1027 candidate, with additional data centers at Brookhaven National Laboratory and the  
1028 NERSC facility as useful additional locations for better redundancy and more efficient  
1029 access to the data from greater number of locations.

1030 **6.2 Collecting and Storing Raw Data**

1031 **6.2.1 Considerations for Event Size Estimates**

1032 To set the scale, let's consider an approximate theoretical **upper limit** on the number of  
1033 channels above the threshold of zero-suppression, for a single track. For this we assume  
1034 digitization rate fixed at 2MHz, and 4312 samples per drift window. In a single anode  
1035 plane assembly (APA), it will be approximately of the order of channel count in the  
1036 APA, i.e. around 2500, *when the track is parallel to the APA plane*. Since each sample is  
1037 16 bit (or 12 bit in more design), we arrive to the limit of approximately 20MB per single  
1038 charged track. For this class of events, the amount of data will scale roughly linearly  
1039 with the length of the track, i.e. in cases when a track is stopped or leaves the sensitive  
1040 volume there will be less data. Further, in most cases the data will be zero-suppressed by  
1041 the front-end electronics (e.g signals below a certain threshold will not be included into  
1042 the outgoing data stream). The exact data reduction factor will depend on a variety of  
1043 factors (cf. threshold), but as a rule of thumb it's an order of magnitude. *We conclude*  
1044 *therefore the events will typically be a few megabytes in size.* This in fact is supported  
1045 by previous Monte Carlo studies performed for earlier versions of LBNE LAr TPC. More  
1046 detail will be presented below.

1047 At the time of writing, work is being done on the physical design of the Liquid Argon  
1048 prototype, and the number of the Anode Plane Assemblies (APA) to be installed in the  
1049 detector is not yet finalized. It will likely be 2 or 3, however there is a possibility of this  
1050 number to be as high as 6. There is therefore a factor of two or three uncertainty in the  
1051 number of readout channels in the detector (e.g. 7680 with 3 APA vs 15360 with 6).

1052 This would affect the amount of data produced by DAQ, although not necessarily by  
1053 a factor of two since a large part of the raw data will be zero-suppressed and occupancy  
1054 in general is expected to be low. With each additional APA, the number of background  
1055 tracks (or track segments) produced by cosmic ray muons will scale very approximately  
1056 at a rate of  $O(1)$  per APA. Because of the direction of incidence of these tracks and  
1057 the fact that in most cases they will be crossing only part of the active volume, we will  
1058 account for this by adding data equivalent to approx. 5 extra tracks to each event. This  
1059 will very roughly correspond the upper limit of 6 APAs in the apparatus and thus the  
1060 estimate will be conservative.

1061 In addition to the principal sensitive volume where Liquid Argon will serve as active  
1062 medium for the TPC, the prototype will also contain a Photon Detector designed to  
1063 record light pulses produced in Argon due to scintillation caused by ionizing radiation.  
1064 In any realistic scenario, the amount of data to be produced by the Photon Detector will  
1065 be quite small compared to that of the Liquid Argon TPC. Same goes for other elements  
1066 of the experimental apparatus (hodoscopes, trigger systems etc) and as a result, for the  
1067 purposes of this section, we shall focus only on the Liquid Argon TPC as the critical  
1068 source of data.

1069 **6.2.2 “Before” and “After” Readout Windows**

1070 As we just mentioned, the detector will be sensitive to background tracks due to cosmic  
1071 ray particles. These must be properly identified and accounted for, in order to ensure  
1072 high quality of the measurements and subsequent detector characterization. Since over-

1073 lay of cosmic ray muons over beam events is stochastic in nature, this can be achieved  
1074 by recording signals which were produced “just before” and “just after” the arrival of  
1075 the test particle from the beamline (this will enable us to reconstruct and account for  
1076 partial or complete background tracks present in the “main” event).

1077 To ensure complete collection of charge due to such tracks, the additional readout  
1078 windows before and after the beam event should equal the nominal total drift time for  
1079 the collection volume (approx. 2.1ms). This will triple the amount of data due to cosmic  
1080 rays, collected from the detector.

### 1081 6.2.3 Statistics and the Volume of Data

1082 Experimental program for the test includes triggering on a few types of particles over  
1083 a range of momenta (see 2.1). We introduce bins for the particle momenta as shown in  
1084 the table below. The estimated event sizes listed in the table are based on Monte Carlo  
1085 studies performed earlier for the 10kt version of the LBNE Far Detector and must be  
1086 considered ballpark estimates. Hadronic and electromagnetic showers were included in  
1087 the MC samples so their effect is accounted for. As a concrete example, for an incident  
1088 electron of 4GeV/c momentum calculations indicate an average event size of  $\sim$ 2MB,  
1089 after zero-suppression.

Particle Type	Momentum Range (GeV/c)	Bin (MeV/c)	Approx. event size, MB
$p$	0.1-2.0	100	1
$p$	2.0-10.0	200	5
$\mu^\pm$	0.1-1.0	50	1
$\mu^\pm$	1.0-10.0	200	5
$e^\pm$	0.1-2.0	100	1
$e^\pm$	2.0-10.0	200	4
$K^+$	0.1-1.0	100	1
$\gamma(\pi^0)$	0.1-2.0	100	1
$\gamma(\pi^0)$	2.0-5.0	200	5

1091 Preliminary plans call for statistics of the order of  $10^4 - 10^5$  events to be collected in  
1092 each bin. Depending on the assumptions, this translates into  $\sim$ 20 million events total  
1093 (for all event classes) to ensure enough statistics for subsequent analysis. Taking into  
1094 account the cosmic ray overlay and additional readout windows as explained in 6.2.2,  
1095 we arrive to a number of  $\sim$ 1PB for total storage space necessary to host **the raw data**.  
1096 This needs to be looked at as the basis for tape budget. As explained below, this volume  
1097 of data needs to be replicated for assured preservation, in at least one more additional  
1098 facility, hence in effect this number must be doubled when budgeting tape.

### 1099 6.2.4 Summary of the Data Volume Estimates

1100 The total amount of data to be collected during the prototype operation will be con-  
1101 siderable under all assumptions and estimates. To fulfill the mission of this test beam  
1102 experiment, we expect that we will need tape storage of  $O(PB)$  size, and a more modest  
1103 disk space for raw data staging at CERN, for replication purposes. We envisage storing

1104 the primary copy of raw data at CERN, with replicas at additional locations. There will  
1105 be additional requirements for processed and Monte Carlo data placement.

### 1106 6.2.5 Raw Data Transmission and Distribution

1107 As mentioned in ??, at least two full replicas will exist for the raw data - at CERN  
1108 and at FNAL (and likely an additional replica at BNL). Moving data outside CERN is  
1109 subject to a number of requirements that include:

- 1110 • automation
- 1111 • monitoring
- 1112 • error checking and recovery (redundant checks to ensure the “precious” data was  
1113 successfully sunk to mass storage at the endpoint)
- 1114 • compatibility with lower-level protocols that are widespread, well understood and  
1115 maintained (cf. gridFTP)

1116 There are a number of systems that can satisfy these requirements, and one of them  
1117 where we possess sufficient expertise and experience is Spade, first used in IceCube [1]  
1118 and then enhanced and successfully utilized in Daya Bay experiment [2].

## 1119 6.3 Databases

1120 A few types of databases will be required:

- 1121 • Run Log, Conditions and Slow Controls records
- 1122 • Offline Calibrations

1123 Databases listed in the former item will need to be local to the experiment in order  
1124 to reduce latency, improve reliability, reduce downtime due to network outages etc. A  
1125 replication mechanism will need to be put in place so the data is readily available at the  
1126 US and other sites. The volume of data stored in these databases will likely to be quite  
1127 modest.

## 1128 6.4 A note on Simulation and Reconstruction Software

1129 Research effort connected to the “Full Scale” prototype at CERN will benefit from  
1130 utilizing simulation toolkits, and tracking and other reconstruction algorithms created  
1131 by communities such as former LBNE, and especially during the 35t test at FNAL. In  
1132 order to leverage this software and expertise, appropriate manpower will need to be  
1133 allocated in order to create and maintain physics analysis tools necessary to fulfill the  
1134 research goals of this experiment.

1135 These tools will rely on software components which will need to be portable, well  
1136 maintained and validated, given the widely distributed nature of the Collaboration and  
1137 the need to use geographically dispersed resources. To ensure that this happens, we  
1138 plan to establish close cooperation among participating laboratories and other research  
1139 institutions. The software will also need to be amenable to running on Grid facilities,  
1140 and will require Distributed Data capability (see 6.5).

1141 **6.5 Distributed Computing, Workload and Workflow Management**  
1142

1143 **6.5.1 Scale of the Processed Data**

1144 According to our estimates, the volume of raw data will be in the petabyte range. The  
1145 offline data can be classified as follows:

- 1146 • Monte Carlo data, which will contain multiple event samples to cover various event  
1147 types and other conditions during the measurements with the prototype detector
- 1148 • Data derived from Monte Carlo events, and produced with a variety of tracking  
1149 and pattern recognition algorithms in order to create a basis for the detector  
1150 characterization
- 1151 • Intermediate calibration files, derived from calibration data
- 1152 • Processed experimental data, which will likely exist in a few branches corresponding  
1153 to a few reconstruction algorithms being applied, with the purpose of their  
1154 evaluation

1155 In the latter, there will likely be more than one processing step, thus multiplying  
1156 data volume. There is sometimes a question about how much of the raw data should be  
1157 preserved in the processed data streams. Given a relatively large volume of raw data, the  
1158 answer in this case will likely be “none” - for practical reasons, meaning that the derived  
1159 data will be just that, and that the size of the processed data will likely be significantly  
1160 smaller than the input (the raw data). Given consideration presented above, we will  
1161 plan for  $\sim$ 1PB of tape storage to keep the processed data. For efficient processing, disk  
1162 storage will be necessary to stage a considerable portion of both raw data (inputs) and  
1163 one or a few steps in processing (outputs).

1164 Extrapolating from our previous experience running Monte Carlo for the former  
1165 LBNE Far Detector, we estimate that we’ll need a few hundred TB of continuously  
1166 available disk space. In summary, we request 2PB of disk storage at FNAL to ensure  
1167 optimal data availability and processing efficiency. Access to distributed data is discussed  
1168 below.

1169 **6.5.2 Distributed Data**

1170 We foresee that data analysis (both experimental data and Monte Carlo) will be per-  
1171 formed by collaborators residing in many institutions and geographically dispersed. In  
1172 our estimates above, we mostly outlined storage space requirements for major data  
1173 centers like CERN and FNAL. When it comes to making these data available to the  
1174 researchers, we will utilize a combination of the following:

- 1175 • Managed replication of data in bulk, performed with tools like Spade discussed  
1176 above. Copies will be made according to wishes and capabilities of participating  
1177 institutions.

- 1178 • Network-centric federated storage, based on XRootD. This allows for agile, just-  
1179 in-time delivery of data to worker nodes and workstations over the network. This  
1180 technology has been evolving rapidly in the past few years, and solutions have been  
1181 found to mitigate performance penalty due to remote data access, by implementing  
1182 caching and other techniques.

1183 In order to act on the latter item, we plan to implement a global XRootD redirector,  
1184 which will make it possible to transparently access data from anywhere. A concrete  
1185 technical feature of storage at FNAL is that there is a dCache network running at this  
1186 facility, with substantial capacity which can be leveraged for the needs of the CERN  
1187 prototype analysis. This dCache instance is equipped with a XRootD “door” which  
1188 makes it accessible to outside world, subject to proper configuration, authentication and  
1189 authorization.

1190 As already mentioned, we plan to host copies of a significant portion of raw and  
1191 derived data at Brookhaven National Laboratory, where substantial expertise exists  
1192 in the field of data handling and processing at scale, due to the principal role this  
1193 Laboratory plays in both RHIC (e.g. STAR) and ATLAS experiments. Initial simple  
1194 tests of XRootD federation to access data residing at FNAL, from a XRootD instance  
1195 located at BNL have been successful. At this point in time we are formulating the  
1196 hardware requirements that need to be fulfilled in order for BNL to play the role of an  
1197 additional data center as described here.

### 1198 6.5.3 Distributed Processing

1199 At the time of writing, FNAL provides the bulk of computational power for LBNE (not  
1200 to mention a few other IF experiments), via Fermigrid and other facilities. We plan to  
1201 leverage these resources to process the prototype data. At the same time, we envisage a  
1202 more distributed computing model where Grid resources are available transparently and  
1203 sometimes on the opportunistic basis, using facilities made available by national Grids  
1204 and in the case of the United States, by the Open Science Grid Consortium.

1205 There are currently very large uncertainties regarding what scale of CPU power will  
1206 be required to process the data, given that tracking, reconstruction and other algorithms  
1207 are in a fairly early stage of development. The best estimates we have at this point range  
1208 from 10 to 100 seconds required by a typical CPU to reconstruct a single event. This  
1209 means that utilizing a few thousand cores through Grid facilities, it will be possible to  
1210 ensure timely processing of these data.

1211 We have not chosen yet the type of Workload Management System to be used for  
1212 the purposes of the CERN prototype test. Currently, many researchers at FNAL are  
1213 using the *jobsub* tool, which opens access to Fermigrid and additionally to the Open  
1214 Science Grid and Cloud resources. There are other capable (and arguably more sophis-  
1215 ticated) system being used, for example by the LHC experiments. We plan to conduct  
1216 an evaluation of these systems with a view to adopt a different solution if necessary.

1217 **7 CERN neutrino platform test environment [5 pages;**  
1218 **David/Jack/Cheng-Ju/Thomas]**

1219 Description of Requirements, layout and constraints

- 1220 • short description of location and orientation of cryostat + cryogenics system in  
1221 EHN1 (David)
- 1222 • description of beam line layout (Cheng-Ju)
- 1223 • space for staging, control room, electronics racks, clean room, scaffolding, etc.  
1224 (Jack)
- 1225 • power requirements and cooling (Jack ?)
- 1226 • ...

1227 **8 Organization, schedule and cost estimate [ $\sim$ 5 pages;**  
1228 **Thomas/Greg]**

1229 insert organization, schedule and cost estimates here

- 1230 • schedule
- 1231 • working group structure and distributions of tasks/responsibilities
- 1232 •
- 1233 • list detector components covered by LBNX project
- 1234 • describe sharing of cryostat responsibilities (engineering, contracting); what is ex-  
1235 pected
- 1236 • beam line expected to be set up by CERN
- 1237 • beam line monitoring
- 1238 • plans for data analysis and publications
- 1239 • describe overlap/commonalities with WA105 data analysis

1240 **9 Summary [ $\sim$ 2 pages; Thomas/Greg]**

1241 this is the summary section

<sub>1242</sub> **References**

<sub>1243</sub> [1] IceCube Data Movement [https://icecube.wisc.edu/science/data/  
datamovement](https://icecube.wisc.edu/science/data/datamovement).

<sub>1245</sub> [2] Data processing and storage in the Daya Bay Reactor Antineutrino Experiment  
<sub>1246</sub> <http://arxiv.org/pdf/1501.06969.pdf>.

<sub>1247</sub> → total estimated page count: ∼60 pages